

Lehigh University Lehigh Preserve

Theses and Dissertations

1-1-1983

Effect of frequency on fatigue crack growth in betaannealed Ti-6Al-4V alloy in 3.5% NaCl solution.

Song Chiou

Follow this and additional works at: <http://preserve.lehigh.edu/etd>



Part of the [Applied Mechanics Commons](#)

Recommended Citation

Chiou, Song, "Effect of frequency on fatigue crack growth in betaannealed Ti-6Al-4V alloy in 3.5% NaCl solution." (1983). *Theses and Dissertations*. Paper 2355.

This Thesis is brought to you for free and open access by Lehigh Preserve. It has been accepted for inclusion in Theses and Dissertations by an authorized administrator of Lehigh Preserve. For more information, please contact preserve@lehigh.edu.

EFFECT OF FREQUENCY ON FATIGUE CRACK GROWTH IN BETA-
ANNEALED Ti-6Al-4V ALLOY IN 3.5% NaCl SOLUTION

by

Song Chiou

A Thesis
Presented to the Graduate Committee
of Lehigh University
in Candidacy for the Degree of
Master of Science
in
Applied Mechanics

Lehigh University

1983

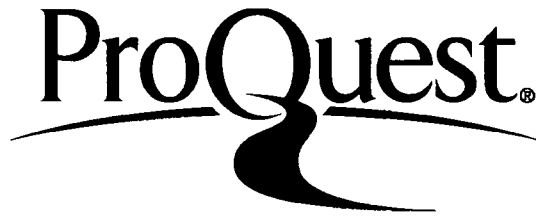
ProQuest Number: EP76631

All rights reserved

INFORMATION TO ALL USERS

The quality of this reproduction is dependent upon the quality of the copy submitted.

In the unlikely event that the author did not send a complete manuscript and there are missing pages, these will be noted. Also, if material had to be removed, a note will indicate the deletion.



ProQuest EP76631

Published by ProQuest LLC (2015). Copyright of the Dissertation is held by the Author.

All rights reserved.

This work is protected against unauthorized copying under Title 17, United States Code
Microform Edition © ProQuest LLC.

ProQuest LLC.
789 East Eisenhower Parkway
P.O. Box 1346
Ann Arbor, MI 48106 - 1346

This thesis is accepted and approved in partial
fulfillment of the requirements for the degree of
Master of Science.

September 14, 1983
(date)

Professor in Charge

Chairman of Department

ACKNOWLEDGEMENT

The author would like to express his gratitude to Professor R. P. Wei who served as his advisor for this research. Dr. Wei's leadership, assistance, along with his personal interest and patience are deeply appreciated. Sincere appreciation is extended to Mrs. Wei for her encouragement and help during this study. Special gratitude to Mr. M. Gao for his invaluable contribution to this study. The author also acknowledges Mr. G. Shim and C. D. Miller for their help with the fracture mechanics experiments. Special gratitude is also extended to Mrs. Simmons for her patiently typing this manuscript.

Support of this research by the Naval Air Development Center, through a subcontract from General Dynamics/Fort Worth, under Contract No. N62269-81-C-0268 is gratefully acknowledged.

Table of Contents

TITLE PAGE	i
CERTIFICATE OF APPROVAL	ii
ACKNOWLEDGEMENT	iii
TABLE OF CONTENTS	iv
LIST OF FIGURES	v
ABSTRACT	1
1. INTRODUCTION	3
2. LITERATURE REVIEW	5
3. MATERIAL AND EXPERIMENTAL WORK	11
3.1 Material and Test Specimens	11
3.2 Test Environment	12
3.3 Experimental Procedure	13
3.4 Crack Length Measurement	15
3.5 Fractography	17
3.6 Microstructure Examination	18
4. RESULT	20
4.1 Fatigue Crack Growth	20
4.2 Fractography and Metallography	23
5. DISCUSSION	27
5.1 The Rate Controlling Process	27
5.2 Role of Hydrides	29
5.3 Brief Discussion of Repassivation and Film Rupture Mechanism	34
6. SUMMARY	36
TABLE AND FIGURES	37
REFERENCES	71
APPENDIX	77
VITA	78

LIST OF FIGURES

<u>Figure</u>		<u>Page</u>
1	Microstructure of Ti-6Al-4V alloy, etched with Knoll's reagent.	38
2	Pole figures for the rolling plane of beta-annealed Ti-6Al-4V alloy plate: (a) (0002) pole, and (b) (10 $\bar{1}$ 0) pole [20].	39
3	Compact tension (CT) specimen.	40
4	Calibration curve of crack length versus normalized compliance for beta-annealed Ti-6Al-4V alloy specimen.	41
5	Calibration curve of crack length versus electrical potential for beta-annealed Ti-6Al-4V alloy specimen.	42
6	Sketch of microstructure work procedure.	43
7	Kinetics of fatigue crack growth in beta-annealed Ti-6Al-4V alloy plate exposed to 3.5% NaCl solution at room temperature (R = 0.05).	44
8	Kinetics of fatigue crack growth in beta-annealed Ti-6Al-4V alloy plate exposed to 3.5% NaCl solution at room temperature (R = 0.3).	45
9	The influence of frequency on fatigue crack growth rate of beta-annealed Ti-6Al-4V alloy in 3.5% NaCl solution at room temperature (R = 0.05).	46
10	The influence of frequency on fatigue crack growth rate of beta-annealed Ti-6Al-4V alloy in 3.5% NaCl solution at room temperature (R = 0.3).	47
11	Kinetics of fatigue crack growth for beta-annealed Ti-6Al-4V alloy plate in vacuum ($p < 10^{-5}$ Pa) at room temperature (R = 0.05).	48

<u>Figure</u>		<u>Page</u>
12	Kinetics of fatigue crack growth for beta-annealed Ti-6Al-4V alloy plate in oxygen ($p = 266 \text{ Pa}$) and in vacuum ($p < 10^{-5} \text{ Pa}$) at room temperature ($R = 0.05$).	49
13	Effect of holding time on kinetics of fatigue crack growth in beta-annealed Ti-6Al-4V alloy plate exposed to 3.5% NaCl solution at room temperature ($R = 0.05$).	50
14	The influence of ΔK on the FSM of beta-annealed Ti-6Al-4V alloy tested in 3.5% NaCl solution at room temperature ($f = 10 \text{ Hz}$ and $R = 0.05$): (a) $16 \text{ MPa-m}^{1/2}$, (b) $27 \text{ MPa-m}^{1/2}$, and (c) $44 \text{ MPa-m}^{1/2}$.	51
15	The influence of frequency on the FSM of beta-annealed Ti-6Al-4V alloy tested in 3.5% NaCl solution at room temperature, $\Delta K = 32 \text{ MPa-m}^{1/2}$ and $R = 0.3$: (a) 10 Hz , (b) 0.3 Hz , and (c) 0.03 Hz .	52
16	Three components of the FSM for beta-annealed Ti-6Al-4V alloy tested in 3.5% NaCl solution: (a) fluted facets, (b) fine striations, and (c) quasi-cleavage with small amount of ductile tearing ($\Delta K = 32 \text{ MPa-m}^{1/2}$, $R = 0.3$).	53
17	SEM fractographs of beta-annealed Ti-6Al-4V alloy tested in 3.5% NaCl solution, showing similar fracture morphology at critical growth rates, (a) $\Delta K = 27 \text{ MPa-m}^{1/2}$ at $f = 10 \text{ Hz}$, (b) $\Delta K = 30 \text{ MPa-m}^{1/2}$ at $f = 3 \text{ Hz}$, and (c) $\Delta K = 44 \text{ MPa-m}^{1/2}$ at $f = 0.3 \text{ Hz}$.	54
18	SEM fractographs of the fluted component of beta-annealed Ti-6Al-4V alloy tested in 3.5% NaCl solution at three different magnifications ($\Delta K = 32 \text{ MPa-m}^{1/2}$, $f = 0.03 \text{ Hz}$, and $R = 0.3$).	55
19	SEM micrographs from mating fracture surfaces of beta-annealed Ti-6Al-4V alloy tested in 3.5% NaCl solution, showing the features of fluted component ($\Delta K = 32 \text{ MPa-m}^{1/2}$, $f = 1 \text{ Hz}$, and $R = 0.3$); mating pairs are a-a' and b-b'.	56

<u>Figure</u>		<u>Page</u>
20	SEM micrographs from mating fracture surfaces of beta-annealed Ti-6Al-4V alloy tested in 3.5% NaCl solution showing the features of striation component ($\Delta K = 32 \text{ MPa-m}^{1/2}$, $f = 10 \text{ Hz}$, $R = 0.3$); mating pairs are a-a' and b-b'.	57
21	Fracture surface profile and the underlying microstructure of beta-annealed Ti-6Al-4V alloy tested in 3.5% NaCl solution ($\Delta K = 44 \text{ MPa-m}^{1/2}$, $f = 0.3 \text{ Hz}$, and $R = 0.05$).	58
22	Fracture surface and the underlying microstructure of beta-annealed Ti-6Al-4V alloy tested in 3.5% NaCl solution ($\Delta K = 44 \text{ MPa-m}^{1/2}$, $f = 0.3 \text{ Hz}$, and $R = 0.05$): (a) fracture surface; (b) section parallel to specimen surface, (c) section transverse to crack growth direction, and (d) fracture surface after etching.	59
23	Fracture surface and the underlying microstructure of beta-annealed Ti-6Al-4V alloy tested in 3.5% NaCl solution ($\Delta K = 44 \text{ MPa-m}^{1/2}$, $f = 0.3 \text{ Hz}$, and $R = 0.05$): (a) fracture surface, (b) section transverse to crack growth direction, (c) section parallel to specimen surface, and (d) fracture surface at a lower magnification.	60
24	Fracture surface and the underlying microstructure of beta-annealed Ti-6Al-4V alloy tested in 3.5% NaCl solution ($\Delta K = 44 \text{ MPa-m}^{1/2}$, $f = 3 \text{ Hz}$, and $R = 0.05$): (a) fracture surface, (b) section parallel to specimen surface, (c) section transverse to crack growth direction, and (d) fracture surface of a higher magnification.	61
25	Schematic illustration of the fracture surface morphology with its underlying microstructure as shown in Fig. 22; angle between alpha platelets and crystallographic (fracture) facet is about 78° .	62

<u>Figure</u>		<u>Page</u>
20	SEM micrographs from mating fracture surfaces of beta-annealed Ti-6Al-4V alloy tested in 3.5% NaCl solution showing the features of striation component ($\Delta K = 32 \text{ MPa-m}^{1/2}$, $f = 10 \text{ Hz}$, $R = 0.3$); mating pairs are a-a' and b-b'.	57
21	Fracture surface profile and the underlying microstructure of beta-annealed Ti-6Al-4V alloy tested in 3.5% NaCl solution ($\Delta K = 44 \text{ MPa-m}^{1/2}$, $f = 0.3 \text{ Hz}$, and $R = 0.05$).	58
22	Fracture surface and the underlying microstructure of beta-annealed Ti-6Al-4V alloy tested in 3.5% NaCl solution ($\Delta K = 44 \text{ MPa-m}^{1/2}$, $f = 0.3 \text{ Hz}$, and $R = 0.05$): (a) fracture surface; (b) section parallel to specimen surface, (c) section transverse to crack growth direction, and (d) fracture surface after etching.	59
23	Fracture surface and the underlying microstructure of beta-annealed Ti-6Al-4V alloy tested in 3.5% NaCl solution ($\Delta K = 44 \text{ MPa-m}^{1/2}$, $f = 0.3 \text{ Hz}$, and $R = 0.05$): (a) fracture surface, (b) section transverse to crack growth direction, (c) section parallel to specimen surface, and (d) fracture surface at a lower magnification.	60
24	Fracture surface and the underlying microstructure of beta-annealed Ti-6Al-4V alloy tested in 3.5% NaCl solution ($\Delta K = 44 \text{ MPa-m}^{1/2}$, $f = 3 \text{ Hz}$, and $R = 0.05$): (a) fracture surface, (b) section parallel to specimen surface, (c) section transverse to crack growth direction, and (d) fracture surface of a higher magnification.	61
25	Schematic illustration of the fracture surface morphology with its underlying microstructure as shown in Fig. 22; angle between alpha platelets and crystallographic (fracture) facet is about 78° .	62

<u>Figure</u>		<u>Page</u>
26	Schematic illustration of the fracture surface morphology with its underlying microstructure as shown in Fig. 24; angle between alpha platelets and crystallographic (fracture) facet is about 79°.	63
27	Schematic illustration of the fracture surface morphology with its underlying microstructure; angle between alpha platelets and crystallographic (fracture) facet is about 78°.	64
28	Comparison between striation spacings and macro crack growth rates at different frequencies.	65
29	Relationship between $(da/dN)_{cf}$ and frequency for Ti-6Al-4V alloy tested in 3.5% NaCl solution at room temperature.	66
30	Relationship between K_{max} and frequency at maximum crack growth rates shown in Fig. 9.	67
31	Fatigue crack growth response for Ti-Al-4V alloy in 3.5% NaCl solution at room temperature ($R = 0.05$) as function of the strain rate parameter $K_{max}^3 \times$ frequency.	68
32	The influence of frequency on fatigue crack growth rate of Ti-6Al-6VSn alloy exposed to 0.6M NaCl solution ($R = 0.1$), by Dawson and Pelloux [11].	69
33	The influence of fatigue crack growth rate of Ti-6Al-4V alloy exposed to 0.6M NaCl solution ($R = 0.1$), by Dawson and Pelloux [11].	70

ABSTRACT

A systematic investigation has been conducted to examine the effect of frequency on fatigue crack growth in a beta-annealed Ti-6Al-4V alloy in 3.5 pct NaCl solution at room temperature. Companion fractographic and metallographic examinations were also made to aid in identifying the probable mechanism for crack growth enhancement (or embrittlement) and for the frequency effect. Fatigue crack growth tests covered a range of frequencies from 0.03 to 15 Hz and a range of K_{\max} levels from about 16 to 61 MPa-m^{1/2}.

The results show that fatigue crack growth rates increased with decreasing frequency, and then decreased with further decreases in frequency. The frequency at which the crack growth rates reached a maximum depended on the K level, and is inversely proportional to $(\Delta K)^3$. The fracture surface morphology also depended strongly on frequency and K level, and suggested that the enhancement of crack growth resulted from the formation and rupture of a hydride phase. Based on the experimental observations, crack growth response is interpreted in terms of control by hydrogen diffusion and of a critical strain

rate required for hydride formation in the crack tip region.

1. INTRODUCTION

Environmental enhancement of fatigue crack growth in metals and high-strength alloys has been well recognized in recent years [1-18]. In a deleterious environment, cyclic load frequency could have an important effect on fatigue crack growth. Most of the systematic work on frequency effect have been carried out on the aluminum alloys and high-strength steels [1-11]. Few studies have been done on titanium and titanium alloys [12-18].

Titanium and titanium alloys are used in a wide range of applications; for instance, in aircraft and ship structures, compressors and turbines, and surgical implants. It is well known that these materials can be susceptible to environmentally enhanced fatigue crack growth (or, corrosion fatigue), and exhibit the attendant effect of frequency. Further understanding of corrosion fatigue crack growth behavior is therefore important to the reliable utilization of titanium and titanium alloys in critical applications.

In this study, Fatigue crack growth experiments were carried out on a beta-annealed Ti-6Al-4V alloy in 3.5 pct NaCl solution to examine systematically the influence of

frequency on crack growth response and to explore the probable mechanisms for the frequency dependence. These experiments are supplemented by detailed microstructural and fractographic examinations. A brief survey of literature is given in Chapter 2 to assess the current state of understanding and to provide a framework for the planned research. Material and experimental procedures are given in Chapter 3. The fatigue crack growth results and the fractographic observations are described in Chapter 4. Implications of these results and probable mechanisms are discussed in Chapter 5. The need for additional work is also discussed.

2. LITERATURE REVIEW

Environmentally assisted subcritical crack growth in structural materials is of great importance, because in many cases these materials are exposed to deleterious environments which can cause embrittlement. The embrittlement sequence involves a number of processes. For a gaseous environment, the processes include gas phase transport, physical adsorption, dissociative chemical adsorption, entry, diffusion and the embrittlement reaction itself (namely, hydrogen embrittlement) [1]. The process that governs subcritical crack growth in a specific material-environment system is dependent on the relative rates of these processes.

Methods to identify the rate controlling process for crack growth have been developed through coordinated fracture mechanics and surface chemistry studies. Experimental results have shown that crack growth under sustained or cyclic load is controlled by gas transport in some cases (e.g., for 2219-T851 aluminum alloy and Ti-5Al-2.5Sn and Ti-6Al-4V alloys in water vapor [2,3], AISI 4340 steel and A542 steel in low pressure hydrogen sulfide [4,5]), or by surface reactions in other cases (e.g., AISI 4340 steel in water or water vapor [6,7] and

in hydrogen [8,9], or by diffusion of hydrogen through the metal in still others (e.g., AISI 4340 steel exposed to a higher pressure of hydrogen sulfide [4]).

A model has been proposed that formalizes the relationship between environmentally assisted fatigue crack growth (or corrosion fatigue) and the gas phase transport and surface reaction processes [10,11]. If the rate of surface reaction is fast relative to the rate of transport, fatigue crack growth is determined by gas transport. (It is to be noted that, in the development of this model, the subsequent processes of diffusion and embrittlement were assumed to be much faster and did not need to be incorporated.) In this case, the model predicts that the corrosion fatigue component of fatigue crack growth rate, $(da/dN)_{cf}$, is a linear function of exposure $(p_o/2f)$, for $p_o/2f$ less than a critical value $(p_o/2f)_s$ (where p_o and f are the gas pressure and loading frequency, respectively). When $p_o/2f$ is equal to and greater than $(p_o/2f)_s$, $(da/dN)_{cf}$ reaches and remains at a saturation value, $(da/dN)_{cf,s}$. These predictions are substantiated by experimental results on 2219-T851 aluminum alloy and Ti-5Al-2.5Sn and Ti-6Al-4V alloys tested in water vapor [2,3] and on A542 steel tested in Hydrogen sulfide [5]. These results tended to support

hydrogen embrittlement as the mechanism for crack growth enhancement [2,5].

Like other structural materials, titanium alloys are often used in aqueous environments, such as sea water. Therefore, it is important to develop an understanding of fatigue crack growth response and to identify the controlling process for crack growth of titanium alloys exposed to aqueous environments. Since the reactions of water with titanium are expected to be very fast, and transport of the environment is not expected to be limiting, other controlling processes for crack growth must be examined. Available experimental data on fatigue crack growth in aqueous environments and on mechanisms of embrittlement are briefly reviewed.

Wanhill [12] observed the effect of frequency on fatigue crack growth for Ti-2.5Cu (IMI230) and Ti-6Al-4V alloys in a 3.5% NaCl solution. The kinetic data showed a significant effect of frequency with rates increasing with decreasing frequency from 50 to 5 Hz. There was no difference in the response between the region above and below K_{ISCC} . The author did not provide a clear cut mechanism of the environmental enhancement of crack growth. They suggested, however, that if environmental

crack growth occurred as a consequence of adsorption, then the effective diffusivity of the absorbed species must be greatly enhanced by the localized plastic deformation at the crack tip.

Meyn [13] studied the effect of frequency on fatigue crack growth rate for Ti-8Al-1Mo-1V alloy in a 3.5% NaCl solution. When K is equal to or above K_{ISCC} , the crack growth rate increased with decreasing frequency. Crack growth rate was independent of frequency below K_{ISCC} . He categorized his data in the $K > K_{ISCC}$ region as type A corrosion fatigue, which was attributed to stress corrosion cracking; and in the $K < K_{ISCC}$ region as type B corrosion fatigue, the "true corrosion fatigue", in which the crack growth rate was independent of frequency. No attempt was made to define the mechanism for corrosion fatigue crack growth.

Dawson and Pelloux [14] investigated frequency effect for Ti-6Al-6V-2Sn and Ti-6Al-4V alloys in a 0.6M NaCl solution. Bucci [15], Döker and Munz [16] performed similar investigations for Ti-8Al-1V-1Sn, Ti-8Al-1Mo-1V and Ti-6Al-4V alloys. Data showed that in the high ΔK region, crack growth rate (da/dN) increased with decreasing frequency. In the intermediate ΔK region, the da/aN

vs. ΔK curves for different frequencies intersected. In the low ΔK region, crack growth rate is independent of frequency. Dawson and Pelloux [14] attributed their data to a competition between repassivation and cyclic stress corrosion cracking. Above K_{ISCC} , corrosion fatigue crack growth was the result of repeated stress corrosion cracking under the applied cyclic loading. Below K_{ISCC} , crack growth rates were determined by the rate of repassivation and the load rise time. Döker and Munz [16] attributed the crack growth behavior in terms of a stress corrosion cracking mechanism. They hypothesized that when $K < K_{ISCC}$, the crack growth rate would be smaller than the propagation rate of the passive film behind the crack tip. The crack propagation was arrested after some time. If K is greater than K_{ISCC} the crack can propagate, but its velocity is limited by the generation rate or the diffusion rate hydrogen, thus leading to a plateau velocity.

Nelson [17] assumed a mechanism of embrittlement of titanium through which hydrogen would reach a sufficiently high level to cause the formation of a brittle hydride. The hydride would accelerate fatigue crack growth or stress corrosion cracking. The crack plane was found to be oriented at 15 degrees from the basal (0001)

plane, which correspondings to a hydride habit plane of $(10\bar{1}7)$ [18].

Pao et al. [19] showed the influence of internal hydrogen on fatigue crack growth by comparing charged specimen data with those of uncharged specimen (530 ppm vs. 53 ppm). The data showed that the growth rates below about 430 K (the hydride stability temperature). They explained the observed behavior in terms of a hydride-embrittlement mechanism.

From the above studies, it can be seen that the frequency effect on fatigue crack growth rates for titanium alloys in aqueous environments is rather complex. There are no consistent explanations for this phenomenon, and the mechanism is still unclear. Diffusion control, repassivation reaction and hydride rupture are considered to be involved in this behavior. To obtain a better understanding, a comprehensive study was undertaken. The main results of this study are given in following sections.

3. MATERIAL AND EXPERIMENTAL WORK

3.1 Material and Test Specimens

A Ti-6Al-4V alloy was chosen for this study. It was received as a 12.7 mm thick plate in the beta-annealed condition. The microstructure of the material consists mainly of colonies or packets of similarly aligned alpha plates with an interplate beta phase. It is usually called coarse Widmanstätten alpha as in Fig. 1. (0002) and (10 $\bar{1}$ 0) pole figures for the rolling plane of the plate are shown in Fig. 2. The rolling texture of the material is very complex. The primary texture has been identified as (10 $\bar{1}$ 3)[$\bar{2}$ 023], in other word, most of the grains are oriented with (10 $\bar{1}$ 3) planes parallel to the rolling plane and with the [$\bar{2}$ 023] and [$\bar{1}$ 2 $\bar{1}$ 0] directions along the rolling transverse directions, respectively.

Compact Tension (CT) specimens were used in this study as shown in Fig. 3. Specimens were prepared in the LT orientation , i.e., with the crack plane perpendicular to the longitudinal direction and crack growth along the long-transverse direction of the plate. A crack starter notch was introduced into each specimen by electrodischarge machining and, subsequently, a 4.4 mm long precrack was introduced at the notch tip by decreasing

load fatigue. This precracking procedure ensured that subsequent fatigue crack growth would be through material that had not been altered by the notch preparation procedure and would be unaffected by the starter notch geometry.

Stress intensity factor K for the CT specimen was computed from Eqn.(1) [21].

$$K = \frac{P(2+\alpha)}{B\sqrt{W}(1-\alpha)^{3/2}} (0.886 + 4.64 \alpha + 13.32 \alpha^2 + 14.72 \alpha^3 - 5.6 \alpha^4) \quad (1)$$

where,

$$\alpha = a/W \quad ; a/W > 0.2$$

P = applied load

B = specimen thickness

W = specimen width

a = crack length

3.2 Test Environment

Fatigue experiments were carried out in vacuum, oxygen and in 3.5% NaCl solution at room temperature. Tests in vacuum were made inside a commercial ultrahigh

vacuum chamber that had been modified to provide mechanical force feed-throughs at pressure below 10^{-5} Pa. Tests in oxygen were made inside the same chamber at an oxygen pressure of 266 Pa.

Tests in 3.5% NaCl solution were made on the immersing the specimen test section in an one-liter solution. The test solution was prepared by dissolving reagent grade NaCl in distilled water, and was continuously purged with nitrogen during each test. The average pH value of the solution was approximately 6.4 at room temperature.

3.3 Experimental Procedure

The crack growth experiments were carried out in an automated closed-loop electrohydraulic testing machine operated in load control. Two different procedures were employed for the fatigue experiments. In the first procedure (procedure A), tests were carried out under constant-amplitude loading at different frequencies. This procedure was used to characterize the crack growth kinetics in either 3.5% NaCl solution or in vacuum. In the second procedure (procedure B) , ΔK was maintained constant by using an automated load shedding method after prescribed numbers of cycles. The constant ΔK procedure

allowed characterization of frequency effects at prescribed ΔK levels in either 3.5% NaCl solution or oxygen.

To examine the effect of hold time, a modified constant ΔK procedure (procedure C) was used. The loading wave form consisted of ramping or linearly increasing K to the selected K_{\max} level, in 0.5s, holding for a prescribed interval, and ramping down to K_{\min} , again in 0.5s. Specimens were tested only in 3.5% NaCl solution.

A step loading technique (procedure D) was used to examine crack growth under static loads. Load was held constant from 30 min to 2 hr in 3.5% NaCl solution, after each incremental increase in load, to establish the absence of detectable crack growth, and was increased by the next increment. If continued crack growth was detected, the load was maintained constant. Otherwise, the load was increased.

Tests corresponding to the different procedures are shown in the test matrices in Table 1.

3.4 Crack Length Measurement

Crack lengths were measured by using either the crack-mouth-opening displacement gage (clip gage) or an a. c. potential system. Calibrations were carried out to establish empirical relationships between crack length and crack-mouth-opening displacement or a.c. potential. Reference marks were made on the specimen surface along the expected crack path and the crack was extended by fatigue in air. When the crack reached a specified length, fatigue loading was interrupted, and a static load was applied and maintained constant. The electrical potential and load-displacement data were recorded. Replicas of the specimen surfaces were made. The actual through-thickness average crack length was measured from replicas, using a travelling microscope, and included a correction for crack front curvature based on post-fracture examinations. The calibration data are shown in Fig. 4 and Fig. 5.

Using the least square method, the normalized potential, compliance and crack length relationships were established. These relationships are given in Eqns. 2 and 3, and also shown in the corresponding figures.

Compliance method (Fig. 4) :

$$a = W(0.9979 - 4.355 U) \quad (\text{in mm}) \quad (2)$$

$$U = \frac{1}{\sqrt{BEV/P} + 1}$$

a = crack length (see Fig. 3)

W = specimen width=63.5 mm (see Fig. 3)

B = specimen thickness

P = applied load

E = Young's modulus

V = crack-mouth-opening displacement

A.c. potential method (Fig. 5) :

$$a = 15.88 + 58.22V^* - 20.69(V^*)^3 \quad (\text{in mm}) \quad (3)$$

$V^* = (V(a) - V_r) / V_r$ = normalized potential

$V(a)$ = potential corresponding the current
crack length

V_r = potential reference corresponding
to the initial notch

Accuracy of crack growth length measurement with the
a.c. potential method was estimated to be better than one

percent for crack length of 20 to 48 mm. The resolution was better than 0.01mm based on 20nV resolution in electrical potential. The error or uncertainty associated with crack length predicted by eqn.(2) for the compliance method was within $\pm 0.8\%$.

3.5 Fractography

The characteristics of fracture surface morphology were observed by scanning electron microscopy. Examinations were made by using the entire broken halves of specimens to avoid artifacts that might be introduced by sectioning, and to provide precise location of areas for correlation with the crack growth data. For selected specimens, both broken halves were placed inside the microscope to allow mating areas of the fracture surfaces to be examined. The scanning electron microscope was operated in the secondary electron imaging mode at 20 KV. A typical working distance of 17 mm was used, and the specimen was tilted at 15 degrees with respect to the incident electron beam about an axis parallel to the direction of crack growth.

3.6 Microstructure Examination

An examination of the fatigue fracture surface in relation to the underlying microstructure was carried out. Two-surface analysis was used to determine the relationship between the microstructure and the fracture surface morphology for selected specimens.

The procedures for preparing the specimen for analysis are as follows (see Fig. 6):

1. A small cubic metallographic sample was cut from the mid-thickness region of one of the broken halves of the specimen by using a diamond cutting wheel. The metallographic sample contains the fracture surface, and exposes sections that are parallel and transverse to the specimen surface.
2. One of these sections (say, one parallel to the specimen surface) was polished and etched. To protect the fracture surface, the sample was mounted with a cool plastic kit. After polishing, the specimen was etched with Kroll's reagent for 60 seconds. The microstructure was revealed and examined by

optical microscopy, with particular attention given to the region close to the fracture surface.

3. The mounting material was then dissolved in Acetone and the specimen was remounted. The second section (say, the transverse section) was polished and etched for examination.
4. The mounting material was dissolved once more. The sample was cleaned carefully and thoroughly, so as not to damage the specimens surfaces (including the fracture surface and the polished surfaces), and was examined by scanning electron microscopy (SEM).
5. The fracture surface was then etched with Kroll's reagent, and the sample was again examined by SEM. By these procedures, relationship between microstructure and surface morphology could be obtained directly.

4. RESULT

4.1 Fatigue Crack Growth

Fatigue crack growth data, obtained from constant load-amplitude fatigue test, are shown in Fig. 7. These data were obtained under sinusoidal loading in 3.5% NaCl solution at a load ratio of 0.05 and at three different frequencies; 10, 3 and 0.3 Hz. The crack growth rate vs. ΔK curves intersect at $\Delta K = 40 \text{ MPa-m}^{1/2}$. When ΔK is below $40 \text{ MPa-m}^{1/2}$, crack growth rates at 10 and 3 Hz are higher than those at 0.3 Hz. Conversely, when ΔK exceeds $40 \text{ MPa-m}^{1/2}$, 0.3 Hz produces the higher crack growth rates.

Similar tests were carried out under constant-amplitude loading with a load ratio of 0.3. The same data trend was observed, Fig. 8. When ΔK is below $30 \text{ MPa-m}^{1/2}$, loading at 10 and 3 Hz produced the highest crack growth rates. Whereas, at ΔK above about $30 \text{ MPa-m}^{1/2}$, fatigue loading at 0.3 Hz resulted in the highest crack growth rate. These results show that the crack growth rate increased with increasing load ratio. This behavior is consistent with a higher mean stress at the higher load ratio [22,23].

To examine the effect of cyclic-load frequency on fatigue crack growth in greater detail, testing was carried out under constant- ΔK loading. Test results for ΔK values of 16, 22, 32, 44, 59 MPa-m^{1/2}, with R=0.05 and frequencies ranging from 15 Hz to 0.03 Hz, are shown Fig. 9. These results show that crack growth rates at each ΔK increased with decreasing frequency, reached a maximum, and then decreased with further decrease in frequency. The frequency corresponding to the maximum crack growth rate increased with decreasing ΔK . Similar results were obtained at $\Delta K = 32$ MPa-m^{1/2}, for a load ratio of 0.3 (see Fig. 10).

Fatigue crack growth rate data obtained in vacuum under constant amplitude loading (Fig. 11) exhibits the same trend as that for 3.5% NaCl solution. To confirm that there is a frequency effect in vacuum, similar tests were carried out under constant ΔK loading in pure oxygen at p=266 Pa. The data showed no essential difference in crack growth rates in vacuum and in oxygen (Fig. 12). The correspondence between the data in vacuum and in pure oxygen implies that there is a frequency effect on crack growth rate in vacuum; (see the discussion section for further development of this implication).

The effect of hold-time, at maximum load, on fatigue crack growth rate are shown in Fig. 13. The crack growth rates are shown as a function of ΔK and hold time, t_h , of 0, 1 and 2.33. Since there is a direct relationship between hold time and frequency, the observed effect on crack growth rate may be attributed to frequency rather than hold time. With zero hold-time, that is, at 1 Hz for the conditions used here, crack growth is slower under triangular wave loading than for sinusoidal loading. This difference is considered in the discussion section.

To determine if sustain-load contributed to the observed enhancement of fatigue crack growth, tests were carried out under constant or sustained load. No detectable sustain load crack growth was observed up to K_{max} 66 MPa-m^{1/2}. Since all the fatigue tests were carried out with K_{max} below 66 MPa-m^{1/2}, no contribution by sustained-load growth or stress corrosion cracking is expected.

4.2 Fractography And Metallography

To assess the influence of environment on the micro-mechanism of crack growth, scanning electron microscopic (SEM) observations of fracture surfaces and of the adjacent metallographic sections were carried out. Typical SEM micrographs of beta-annealed Ti-6Al-4V alloy specimen tested in 3.5% NaCl solution at room temperature are shown in Figs. 14 and 15. Figure 14 shows the variation of surface morphology with K level, whereas Fig. 15 shows changes with test frequency. Three different components may be identified; namely, (i) flutes [24], (ii) fine striations, and (iii) quasi-cleavage with small amount of ductile tearing [25]. These components are shown at higher magnifications in Figs. 16 to 20. The relationship of fracture surface morphology with the underlying microstructure is illustrated by the SEM micrographs and the accompanying sketches in Figs. 21 to 27.

The first component is composed of facets containing colonies of rod-like elements (or flutes), and represents crack growth across colonies of similarity aligned and crystallographically oriented alpha-platelets (see Figs. 14, 15, 16a and 17) [24]. The areal fraction of this component increased with increasing K. It also increased with decreasing frequency at first, but then decreased

with further reductions in frequency. The greatest amount of this component corresponded to the frequency at which the fatigue crack growth rate is a maximum at a given K level (see Figs. 17 and 18).

More detailed examinations indicate that the direction of flutes are nearly parallel to the traces of alpha-platelets on the fracture surfaces (Fig. 18). Fatigue striations were also observed which are nearly parallel to the axis of the flutes, with the local growth direction nearly perpendicular to the flute axis. Figure 19, taken from mating fracture surfaces, shows patches of fluted regions that intersect with regions that contain fatigue striations. These microfractographs show that flutes, which were once mistaken for cleavage, striations or river patterns, are the result of internal necking [26]. The flutes are likely to be the nucleation sites of titanium hydrides, although no evidence of hydride was found on the fracture surface.

The second component appears as nearly flat facets (region A in Figs. 14 and 15) or as intergranular fracture (region B in Figs. 14 and 15), and was nearly absent at the frequency for maximum enhancement of crack growth

at a given K level. Examinations at higher magnifications show that the facets are covered with very fine striations (see Fig. 16b and microfractographs of mating surfaces in Fig. 20). The spacing of the striations is several times smaller than the corresponding macroscopic crack growth rate, Fig. 28. These facets appear to correspond to growth along the prior beta grain boundaries or through alpha-phases that are formed along these boundaries, Fig. 20. It is interesting to note that the striations appear to be ductile on one surface, and to have a very different and brittle appearance on the mating surface. This is caused by the fact that the slip system in this hcp alloy is limited.

The remaining component is quasi-cleavage with a small amount of ductile tearing [25]. This component may be seen in the SEM microfractographs at the high and low frequencies, and was nearly absent at frequencies where the environmental effect was highest (see Figs. 14, 15, 17).

The relationship between the fracture surfaces and the underlying microstructure are shown in Figs. 21 to 27. Using a two-surface trace analysis technique, the angles between the striated and fluted fracture facets

and the underlying alpha-platelets were found to be approximately 78 degrees. This characteristic value implies that hydrogen assisted fatigue crack growth may result from the formation and rupture of titanium hydride [18]. The possibility of hydride formation and its role in explaining the observed frequency dependence for fatigue crack growth is considered in the next section.

5. DISCUSSION

The results show that the effect frequency on fatigue crack growth in beta-annealed Ti-6Al-4V alloy in 3.5% NaCl solution is complex. To understand the observed response, it is useful to recall the concepts developed for gaseous environments [1-8]. There, the processes for enhancing crack growth included transport of the deleterious gas to the crack tip, reactions of the gas with newly created surfaces at the crack tip to evolve hydrogen, diffusion of hydrogen into a region ahead of the crack tip to produce embrittlement, and the embrittlement reaction itself. The actual crack growth rate is determined by the rate controlling process and the embrittlement mechanism [27]. It is reasonable to consider the crack growth response within this context, where in a transfer of control or a change in mechanism may take place with changes in frequency.

5.1 The Rate Controlling Process

To study the frequency effect on crack growth rate for Ti-6Al-4V in 3.5% NaCl solution, the first step is to determine which is the rate controlling process. Because of the presence of liquid at the crack tip, the transport

process is not considered to be limiting. Surface reactions with water vapor have been measured and are found to be extremely rapid [3]. Hence, reactions of 3.5% NaCl solution with this alloy are not expected to be the controlling process. The most likely rate controlling process, therefore, is either that of hydrogen diffusion into the titanium alloy or the embrittlement reaction.

A number of models for diffusion controlled crack growth rate have been proposed [4,28]. The models predict that the crack growth rates would vary according to the square root of time and diffusivity, with an activation energy equal to one-half of that for diffusion. In other words the cycle-dependent component of fatigue crack growth rate, $(da/dN)_{cf}$, should be a function of $(1/\text{frequency})^{1/2}$ [29] (see Eqn. 1). The crack growth rates in oxygen and in vacuum were used as reference in computing $(da/dN)_{cf}$. Interpolation was used to estimate the reference crack growth rate for the corresponding conditions of ΔK and frequency utilized for the tests in 3.5% NaCl solution. The results are shown as $\log((da/dN)_{cf})$ vs $\log(1/\text{frequency})$ in Fig. 29 for the region where the crack growth rates increased with decreasing frequency.

The slope over this region was found to be 0.48 ± 0.04 (at the 95% confidence level) by statistical analysis of the pooled results. This slope is consistent with that for hydrogen diffusion, and suggests that the rate controlling process at the higher frequencies is that of hydrogen diffusion into a region of the material ahead of the crack tip. This identification, however, is not sufficient to account for the decreases in crack growth rates with further decreases in frequency and for the effect of K level on the frequency dependence.

5.2 Role Of Hydrides

One plausible explanation for the data trend shown in Fig. 9 is that the enhancement of crack growth resulted from the formation and rupture of titanium hydrides, which can be dependent on strain rate. Support for hydride formation and rupture is provided by the results of Peterson [30] and Pao [19,31,32]. Peterson showed that hydrogen embrittlement can occur even in vacuum at 1.33×10^{-8} Pa and attributed its cause to hydrides formed by internal hydrogen [30]. Pao showed that crack growth rates were increased by increasing the concentration of dissolved hydrogen in titanium alloys, and were reduced substantially when the test temperature was increased above which hydrides ceased to be stable

[19,31,32]. He explained these results in terms of a hydride mechanism for embrittlement.

Further support for hydride formation and rupture is provided by the measurement of planar angle between fracture surface and alpha-platelets described in the previous section. The angle between the fluted facets and the alpha-platelets has been determined to be 78 degrees by using two surface trace analysis. This result is comparable with the angle between hydride habit plane (10 $\bar{1}$ 7) [18] and alpha-platelets (i. e. between 75.3 and 82.8 degrees, see Appendix I). There is, however, no direct evidence for hydrides from this study.

In addition, indirect support is also provided through the crack growth behavior in vacuum and in oxygen, Figs. 11 and 12. These results show a frequency effect on crack growth rate; although not as pronounced as that observed in the 3.5% NaCl solution.

From the above discussion, one may suggest that hydride formation and rupture could be considered as the embrittlement mechanism.

The fact that hydride formation is sensitive to strain rate has been shown by a number of investigators [36-39]. At low hydrogen concentrations, the strain rate will aid in overcoming the barrier and enhance hydride formation [40]. It was also found that hydride embrittlement became more severe with increased strain rate [38,41,42].

For the beta-annealed Ti-6Al-4V alloy used in this study, with a low hydrogen concentration, it is reasonable to assume that the observed crack growth response resulted from the strain rate dependence for hydride formation. At the higher strain rates, or higher test frequencies, the material would appear to be brittle because of hydride formation. At the lower frequencies or strain rates, the material would be more ductile with little or no hydride present. The more brittle states would result in high crack growth rates than the more ductile states. There is a "critical value" of strain rate or a "critical" frequency at each K level below which no hydride would be formed. Crack growth rate reaches a maximum at this frequency, and is expected to decrease abruptly below this critical frequency.

The fracture surface morphology supports the proposed explanation, Figs. 14, 15, 17. In the high frequency region, striations and some fluted components are present. The fluted component, which is believed to be associated with hydride formation and rupture, increased with decreasing frequency. At the critical frequency of corresponding crack growth rate point, the fracture surface is largely covered with the fluted component Fig. 15. Below this frequency, the fluted component nearly disappears and the material appears to be ductile. These observations are consistent with the dependence of hydride formation on strain rate.

For the critical strain rate concept to be valid, a unique relationship between critical frequency and K level must exist. In other words, the critical points of highest crack growth rate in all of the K levels must have the same strain rate. The data were analyzed on the basis of this assumption and are shown in Fig. 30. The results show that the condition of constant "critical" strain rate is met by having the product $(K_{\max})^3 \times (\text{frequency})$ equal to a constant. The crack growth data were replotted as (da/dN) vs. $(K_{\max})^3 \times (\text{frequency})$ in Fig. 31, and show good agreement among the data at the various K levels. The theoretical

strain rates based on linear elasticity and on the elastic-plastic analysis proposed by Hilton, Hutchison and Rosengren [43,44], however, suggest that either $(K_{\max}) \times (\text{frequency})$ or $(K_{\max})^2 \times (\text{frequency})$ should be constant. Additional analytical study is needed to clarify this issue.

The effect of frequency on crack growth rate for beta-annealed Ti-6Al-4V alloy in 3.5% NaCl solution, therefore, can be explained in terms of diffusion control and a strain-rate dependent hydride formation mechanism. In the region where crack growth rate increases with decreasing frequency, the crack growth rate is controlled by hydrogen diffusion, such that $(da/dN)_{cf}$ shows a dependence on $(1/\text{frequency})^{1/2}$, and is determined by hydride formation and rupture. When the frequency is decreased below the critical frequency, the material becomes more ductile, with little or no hydride formation, and the crack growth rate decreased abruptly. It is expected that the crack growth rate would still be controlled by hydrogen diffusion, and resume the $(1/\text{frequency})^{1/2}$ dependence at sufficiently low frequencies.

5.3 Brief Discussion Of Repassivation And Film Rupture Mechanism

Dawson, Pelloux and Döker, and Munz [14,16] have studied the effect of frequency on crack growth rate for titanium alloys in halid solutions, and had obtained similar results (see Introduction). They proposed to explain their results in terms of a film repassivation and rupture mechanism over the entire frequency range. For this explanation to apply, $(da/dN)_{cf}$ must be inversely proportional to frequency (assuming repassivation follows first-order reaction kinetics) and the repassivation time must be consistent with the range of frequencies where environmental effects are observed. Their data were reanalyzed by using the same superposition model utilized in this study and are shown in Figs. 32 and 33. The results show that $(da/aN)_{cf}$ is again a function of $(1/\text{frequency})^{1/2}$ instead of $1/\text{frequency}$. The repassivation time was measured to be of the order of 10^{-3} second for titanium alloys in halid solutions [45,46]. This time is 2 to 4 orders of magnitude lower than that encountered in fatigue, i.e., corresponding to frequencies from 10^{-1} to 10 Hz. (about 10 to 10^{-1} second) Consequently, an explanation using a repassivation and film rupture mechanism cannot be applied, and the hydride

mechanism, diffusion control and strain rate effect appears to be more reasonable.

6. SUMMARY

The frequency effect on crack growth rate for beta-annealed Ti-6Al-4V alloy in 3.5% NaCl solution has been examined. The results show that the crack growth rate at a given ΔK increased with decreasing frequency, reached a maximum, and then decreased with decreasing frequency. Diffusion control is considered to be the rate controlling process. Enhancement of crack growth is attributed to hydride formation and rupture, which is dependent on strain rate. The observed frequency effect is explained in terms of diffusion control in conjunction with a strain rate dependent hydride embrittlement mechanism. This explanation is supported by analyses of fracture morphology and crack path in relation to the alloy microstructure. The frequency at which a maximum in crack growth rate is obtained at a given K level is given by the relationship $(K_{\max})^3 \times \text{frequency} = \text{constant}$. Further studies should be pursued in the following area:

1. Obtaining direct evidence of hydride formation during crack growth.
2. Understanding of the relationship between the hydride formation and strain rate.
3. Calculation of crack-tip strain rate.

PROCEDURE A

Envir. →		Vacuum	3.5% NaCl
Freq. (Hz)	10	--	* o
	5	*	--
	3	--	* o
	1	*	--
	0.3	--	* o
	0.1	*	--

* --- load ratio, R = 0.05

o --- load ratio, R = 0.3

PROCEDURE C

Envir. →		3.5% NaCl				
ΔK (MPa-m ^{1/2})		25	30	38	43	51
Holding time (s)	0	*	*	*	*	*
	1	*	*	*	*	*
	2.33	--	*	*	*	*

* --- load ratio, R = 0.05

o --- load ratio, R = 0.3

PROCEDURE B

Envir. →		Oxygen (p = 266 Pa)					3.5% NaCl				
ΔK (MPa-m ^{1/2}) →		16	26	32	44	59	16	22	32	44	59
Freq. (Hz)	15	--	--	--	--	--	*	*	*	--	--
	10	--	--	--	--	--	*	*	**o	**	*
	8	*	--	--	--	--	--	--	--	--	--
	5	--	*	--	--	--	--	--	*	--	--
	3	--	--	*	*	*	*	*	**o	**	*
	1.6	--	--	--	--	--	--	--	*	--	--
	1	--	*	*	*	*	*	*	**o	**	*
	0.6	--	--	--	--	--	--	--	*	--	--
	0.5	--	--	--	--	--	--	--	--	*	*
	0.3	--	--	*	*	*	*	*	**o	**	*
	0.1	--	--	*	*	--	--	*	**o	**	*
	0.03	--	--	*	*	--	--	--	**o	**	--

* --- load ratio, R = 0.05

o --- load ratio, R = 0.3

PROCEDURE D

$$K_{\max} = 66 \text{ MPa-m}^{1/2}$$

TABLE 1: Table listing of the test procedures.

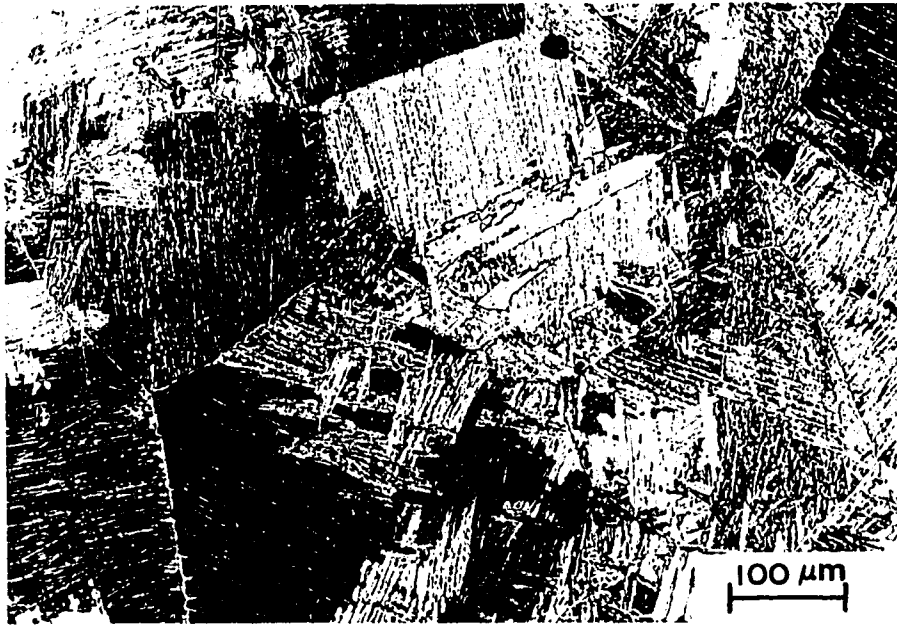


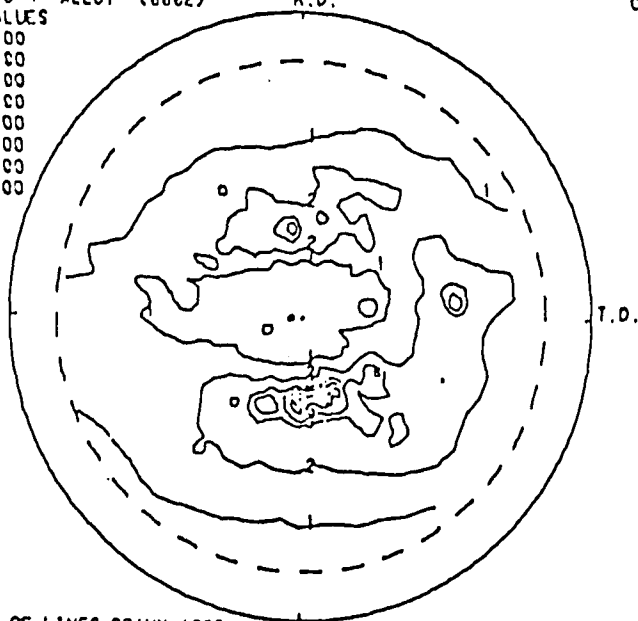
Figure 1: Microstructure of Ti-6Al-4V alloy, etched with Kroll's reagent.

30-1 11-6-4 ALLOY (0002)

R.D.

CONTOUR VALUES

1	3.00
2	5.00
3	8.00
4	10.00
5	13.00
6	15.00
7	18.00
8	23.00



TOTAL NO. OF LINES DRAWN-1287

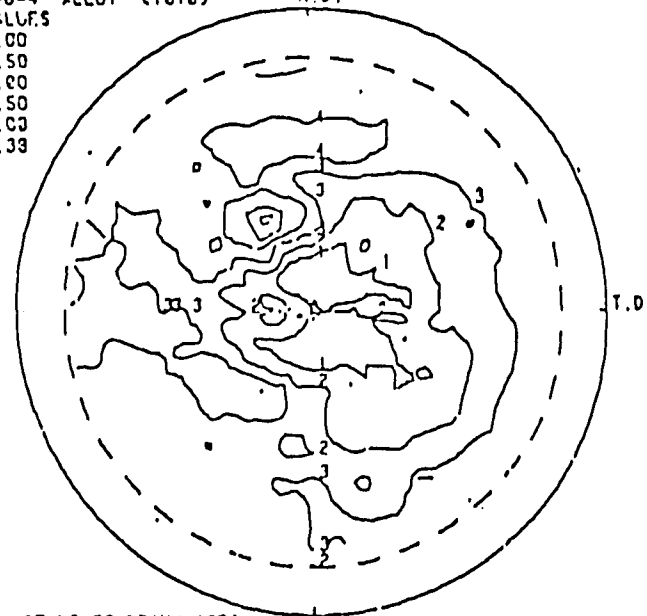
(a)

PG4 11-6-4 ALLOY (1010)

R.D.

CONTOUR VALUES

1	2.00
2	2.50
3	3.00
4	3.50
5	4.00
6	4.38



TOTAL NO. OF LINES DRAWN-1383

(b)

Figure 2: Pole figures for the rolling plane of beta-annealed Ti-6Al-4V alloy plate: (a) (0002) pole, and (b) (1010) pole [20].

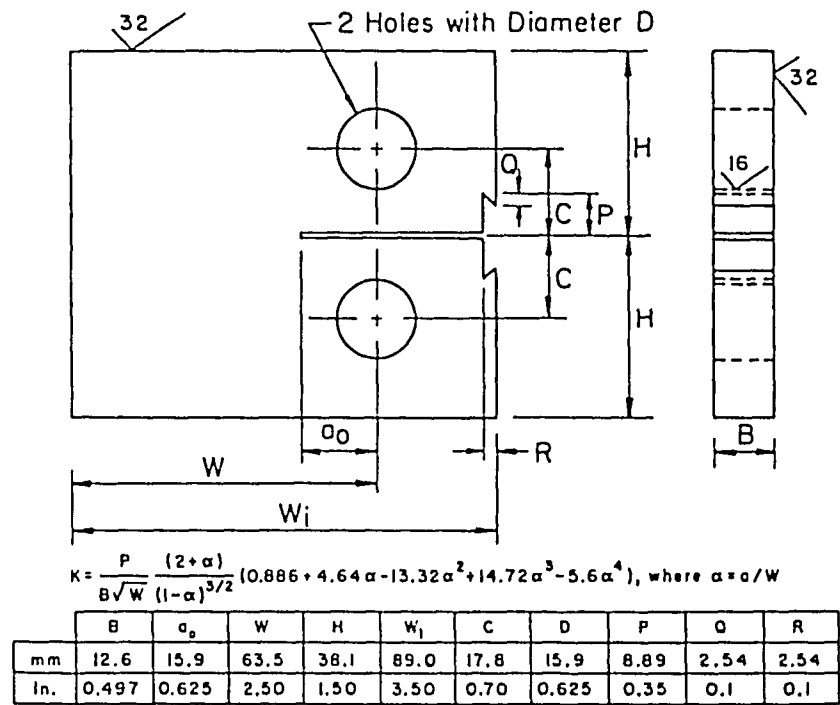


Figure 3: Compact tension (CT) specimen.

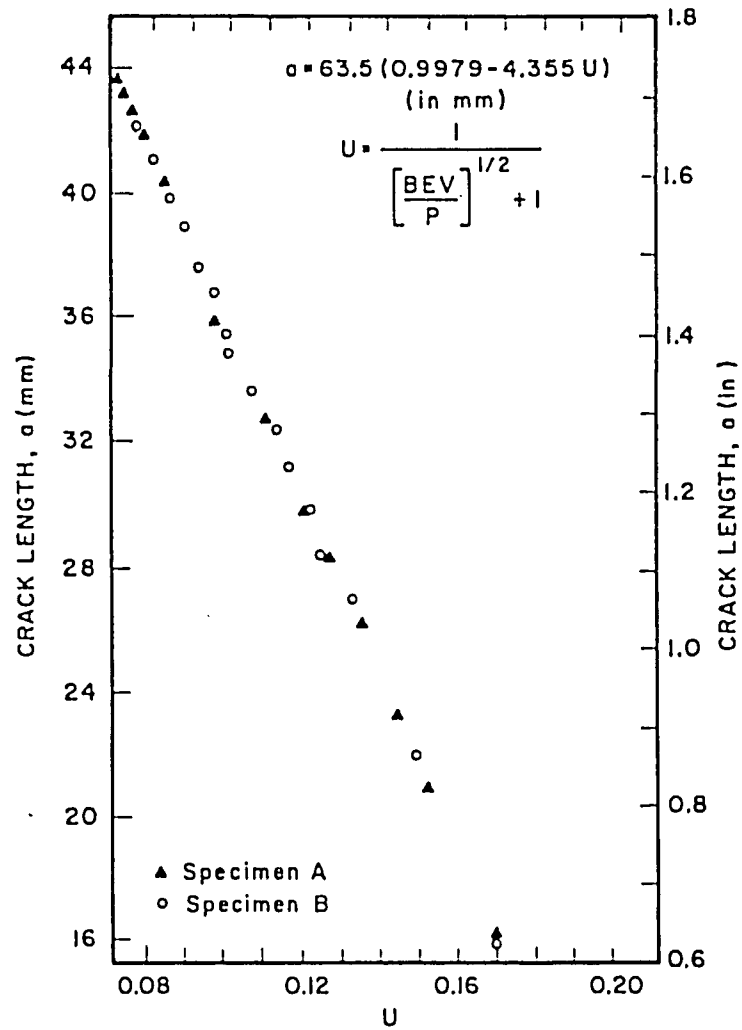


Figure 4: Calibration curve of crack length versus normalized compliance for beta-annealed Ti-6Al-4V alloy specimen.

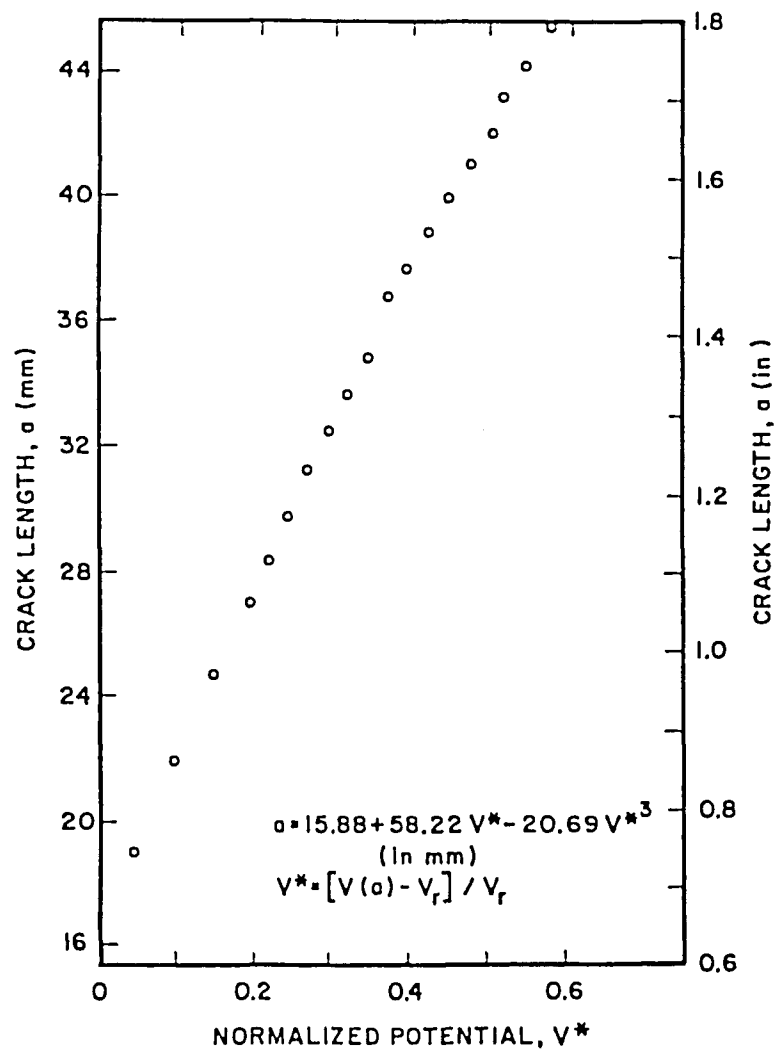


Figure 5: Calibration curve of crack length versus electrical potential for beta-annealed Ti-6Al-4V alloy specimen.

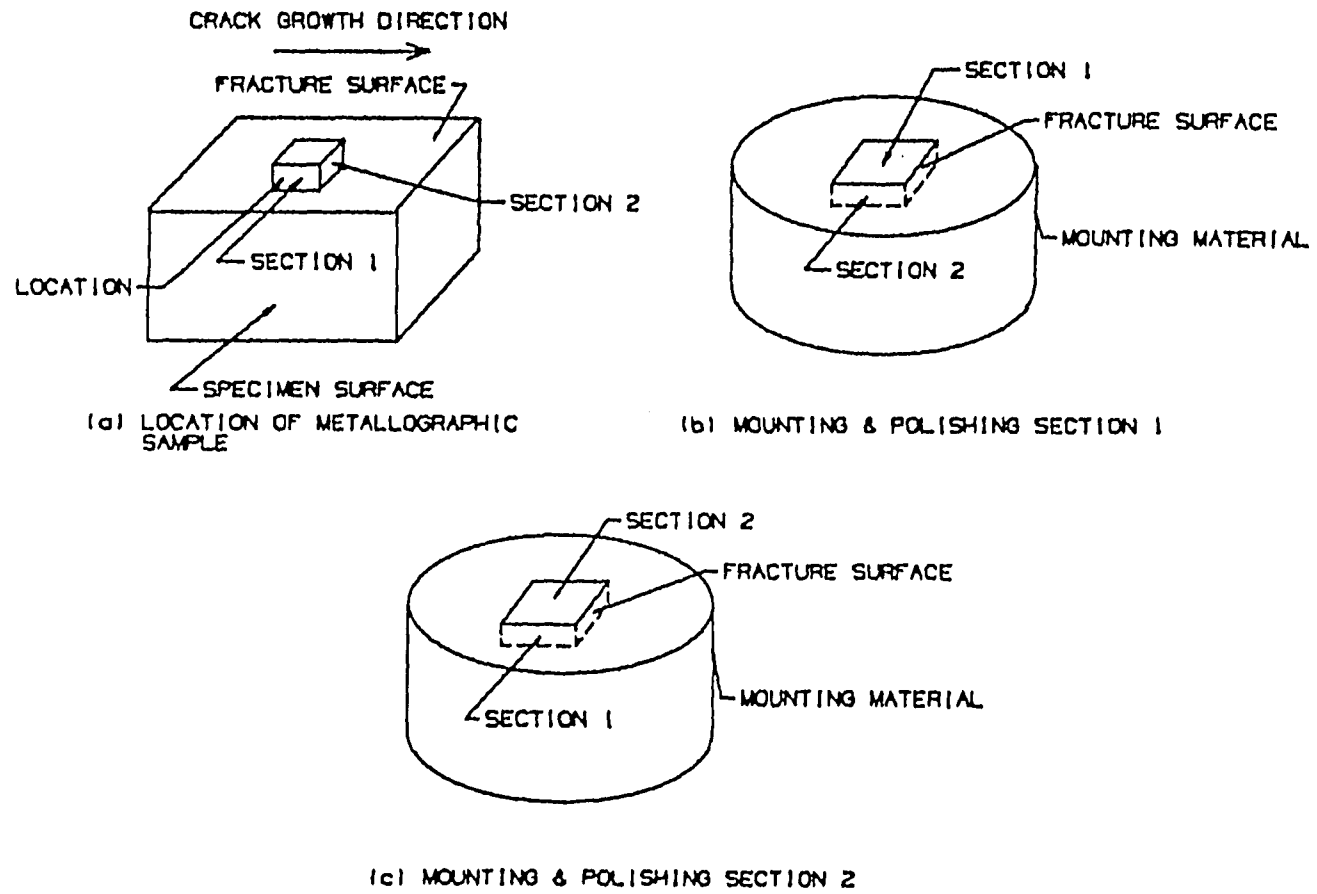


Figure 6: Sketch of microstructure work procedure.

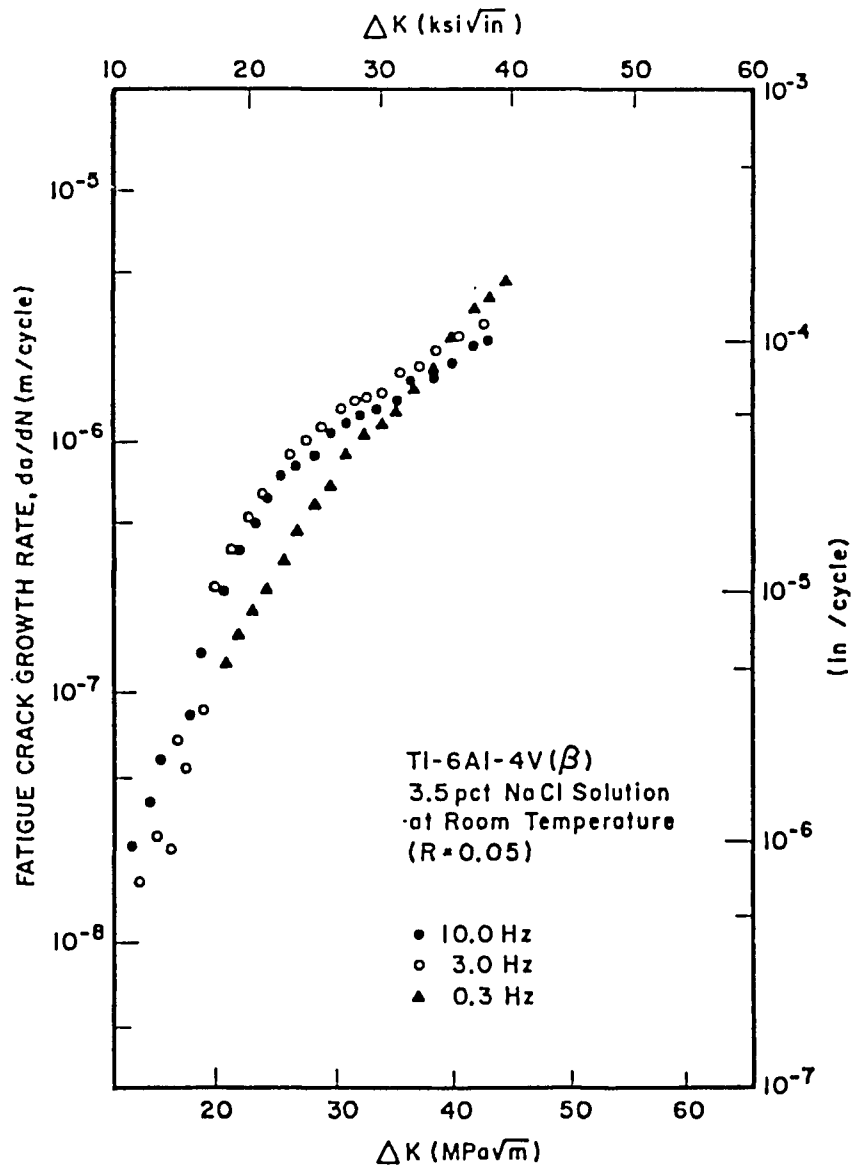


Figure 7: Kinetics of fatigue crack growth in beta-annealed Ti-6Al-4V alloy plate exposed to 3.5% NaCl solution at room temperature (R = 0.05).

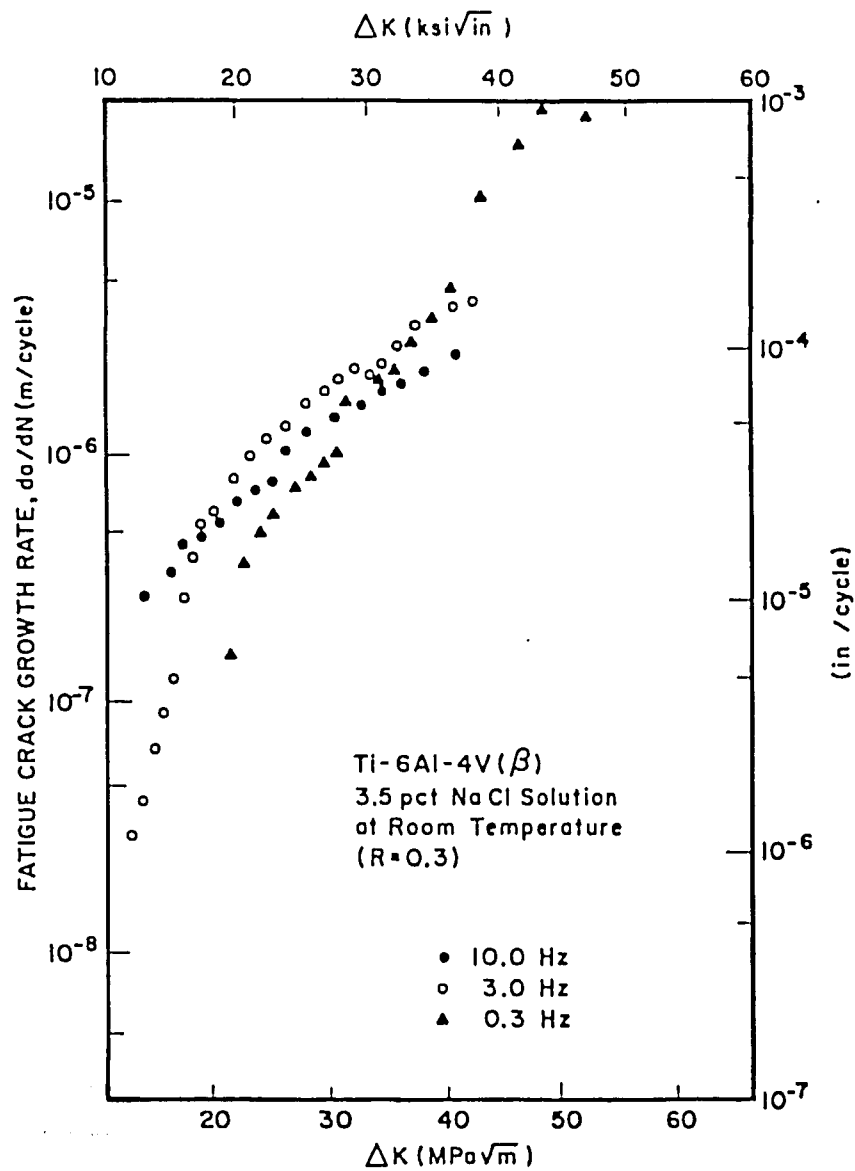


Figure 8: Kinetics of fatigue crack growth in beta-annealed Ti-6Al-4V alloy plate exposed to 3.5% NaCl solution at room temperature (R = 0.3).

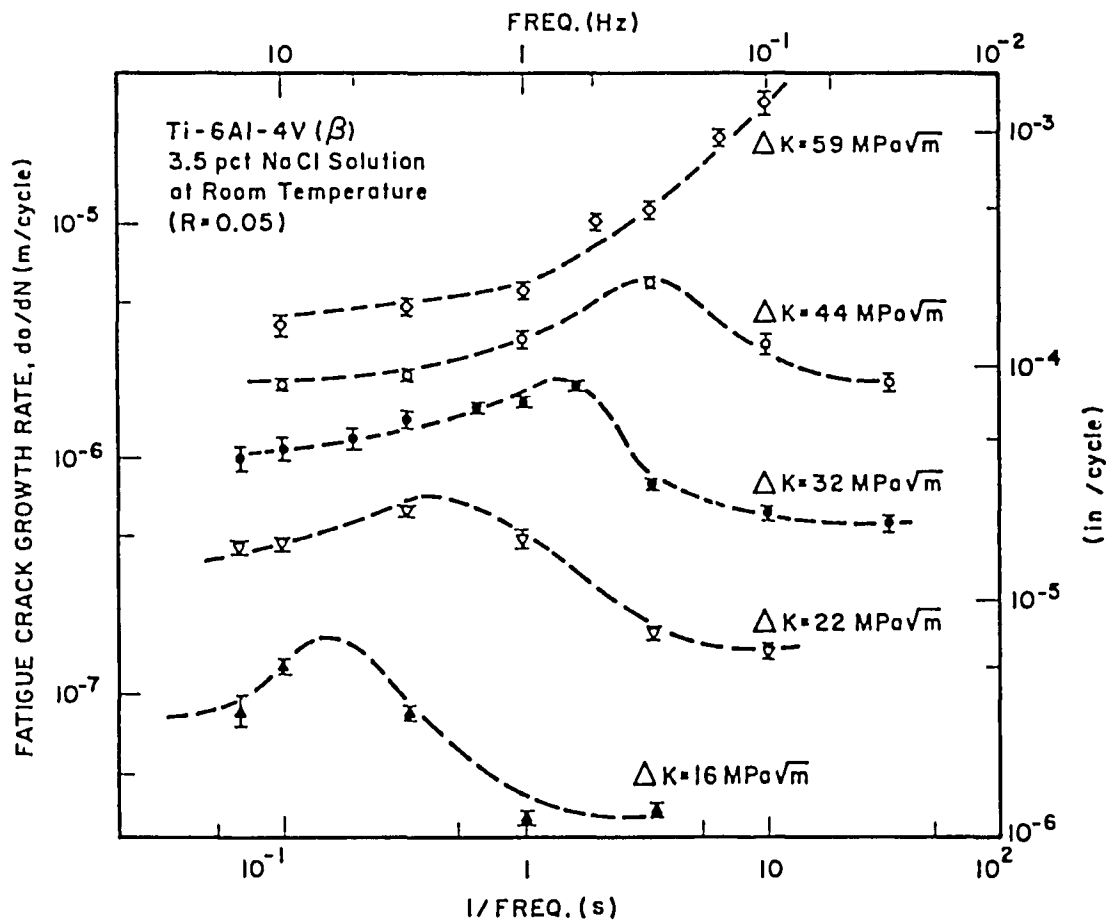


Figure 9: The influence of frequency on fatigue crack growth rate of beta-annealed Ti-6Al-4V alloy in 3.5% NaCl solution at room temperature ($R = 0.05$).

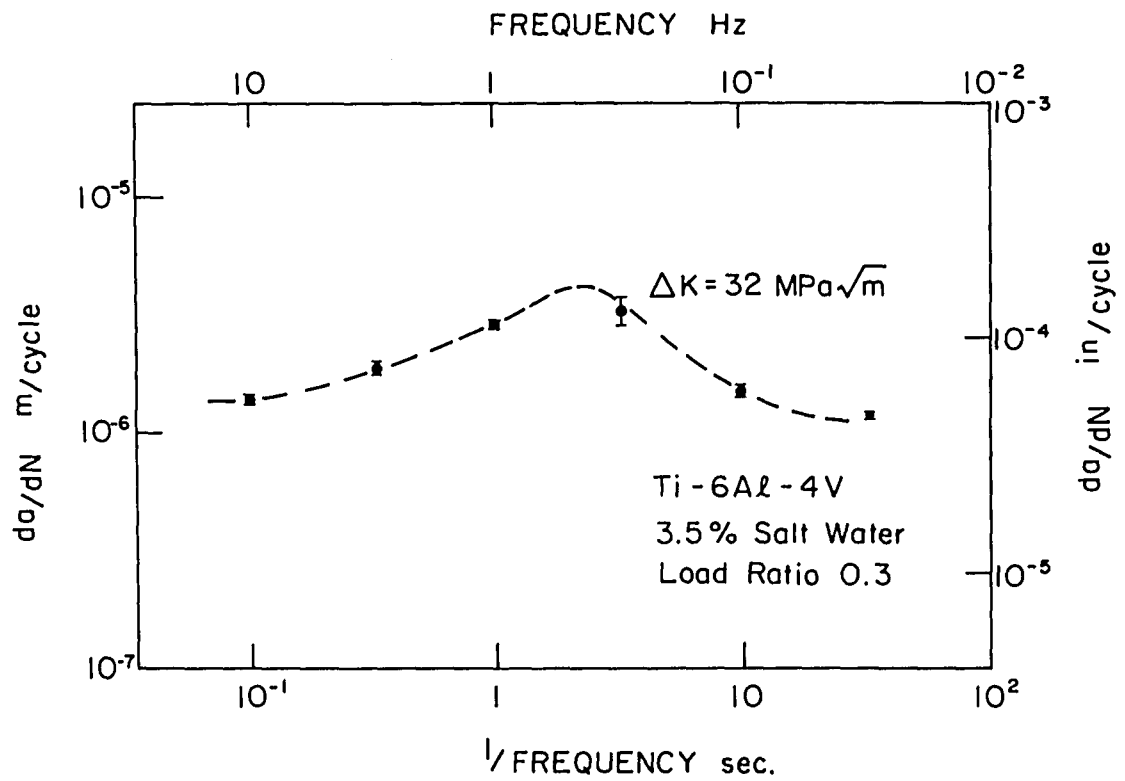


Figure 10: The influence of frequency on fatigue crack growth rate of beta-annealed Ti-6Al-4V alloy in 3.5% NaCl solution at room temperature ($R = 0.3$).

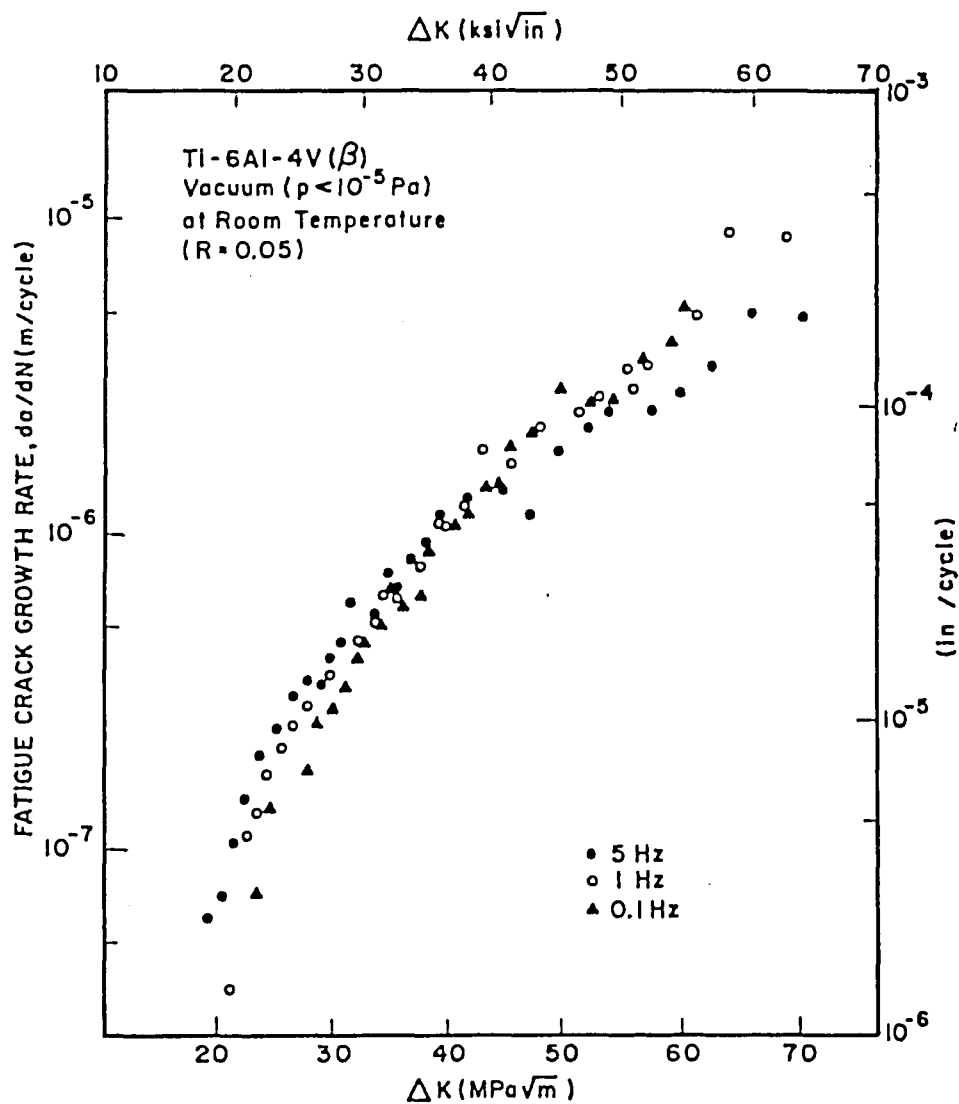


Figure 11: Kinetics of fatigue crack growth for beta-annealed Ti-6Al-4V alloy plate in vacuum ($p < 10^{-5}$ Pa) at room temperature ($R = 0.05$).

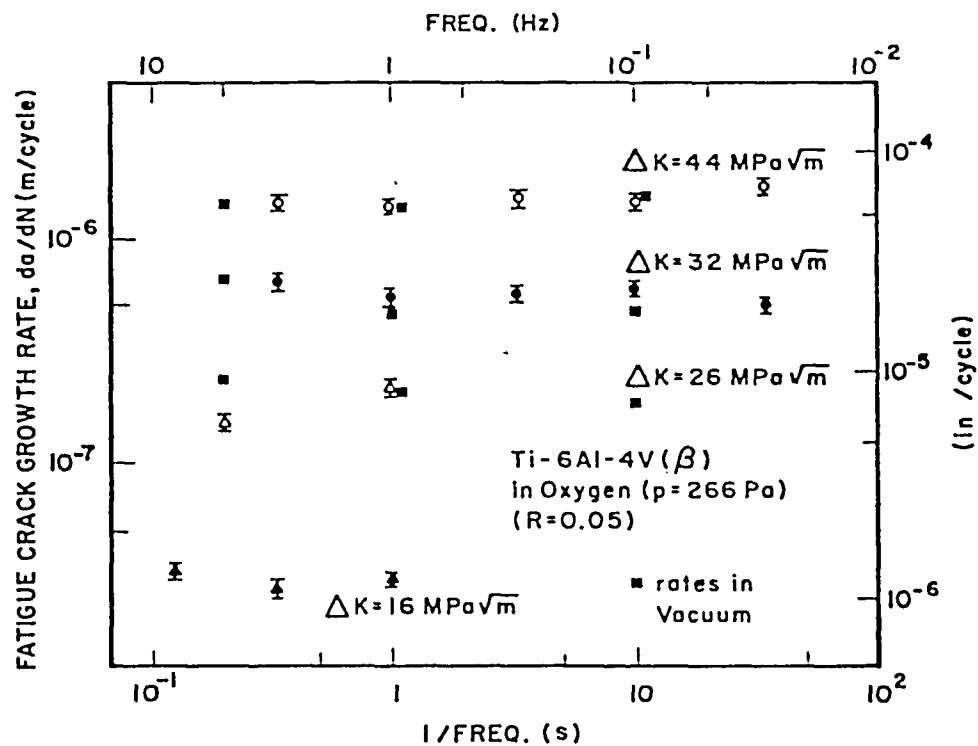


Figure 12: Kinetics of fatigue crack growth for beta-annealed Ti-6Al-4V alloy plate in oxygen ($p = 266$ Pa) and in vacuum ($p < 10^{-5}$ Pa) at room temperature ($R = 0.05$).

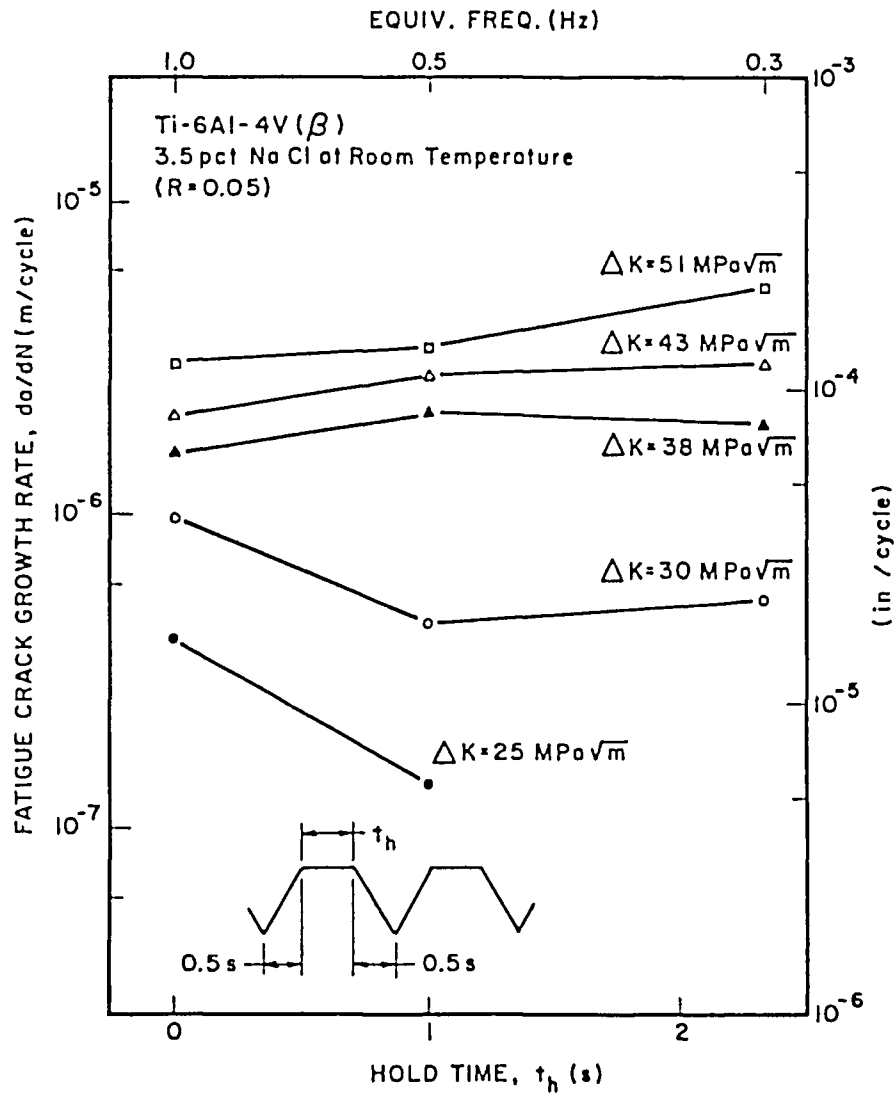


Figure 13: Effect of holding time on kinetics of fatigue crack growth in beta-annealed Ti-6Al-4V alloy plate exposed to 3.5% NaCl solution at room temperature ($R = 0.05$).

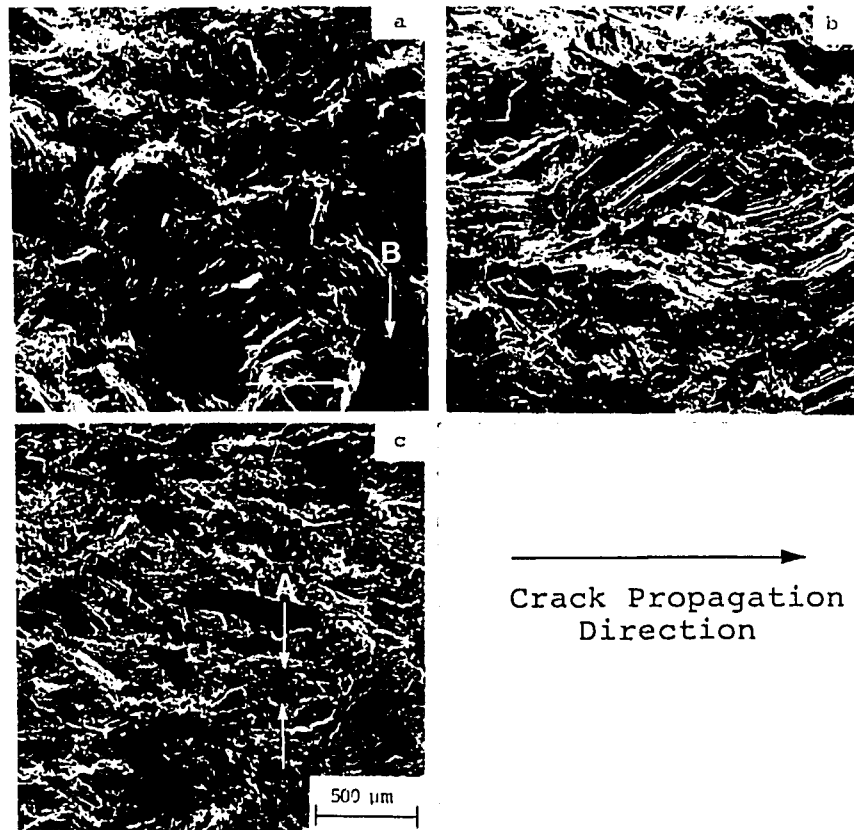


Figure 14: The influence of ΔK on the FSM of beta-annealed Ti-6Al-4V alloy tested in 3.5% NaCl solution at room temperature ($f = 10$ Hz and $R = 0.05$): (a) $16 \text{ MPa}\cdot\text{m}^{1/2}$ (b) $27 \text{ MPa}\cdot\text{m}^{1/2}$, and (c) $44 \text{ MPa}\cdot\text{m}^{1/2}$.

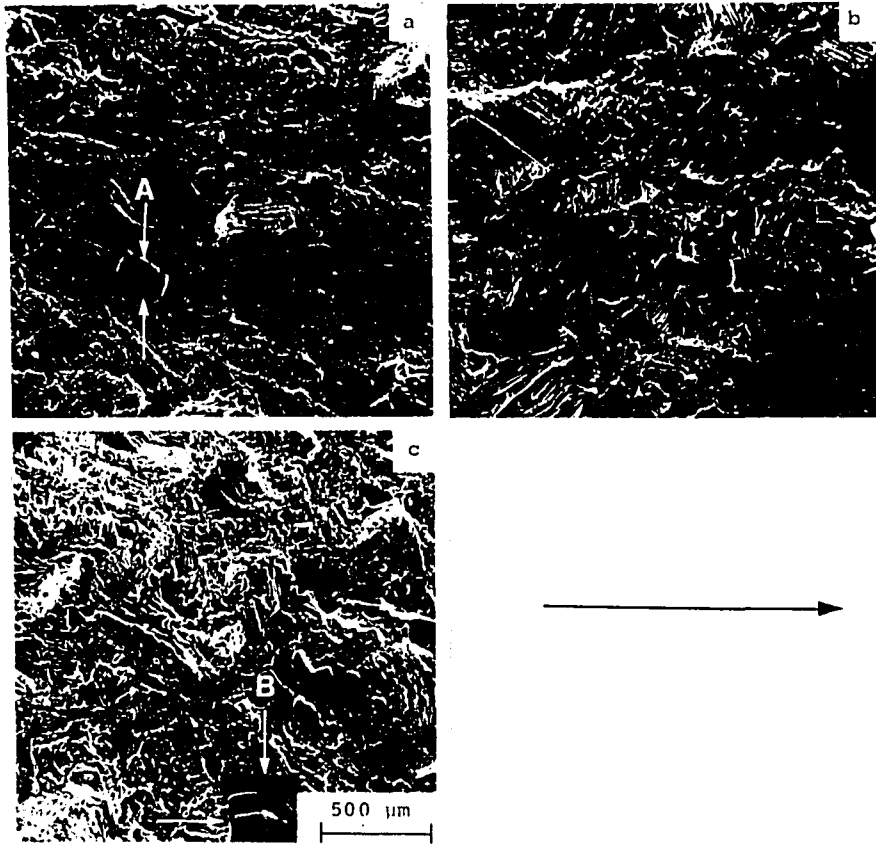


Figure 15: The influence of frequency on the FSM of beta-annealed Ti-6Al-4V alloy tested in 3.5% NaCl solution at room temperature, $\Delta K = 32 \text{ MPa}\cdot\text{m}^{1/2}$ and $R = 0.3$:
(a) 10 Hz, (b) 0.3 Hz, and (c) 0.03 Hz.

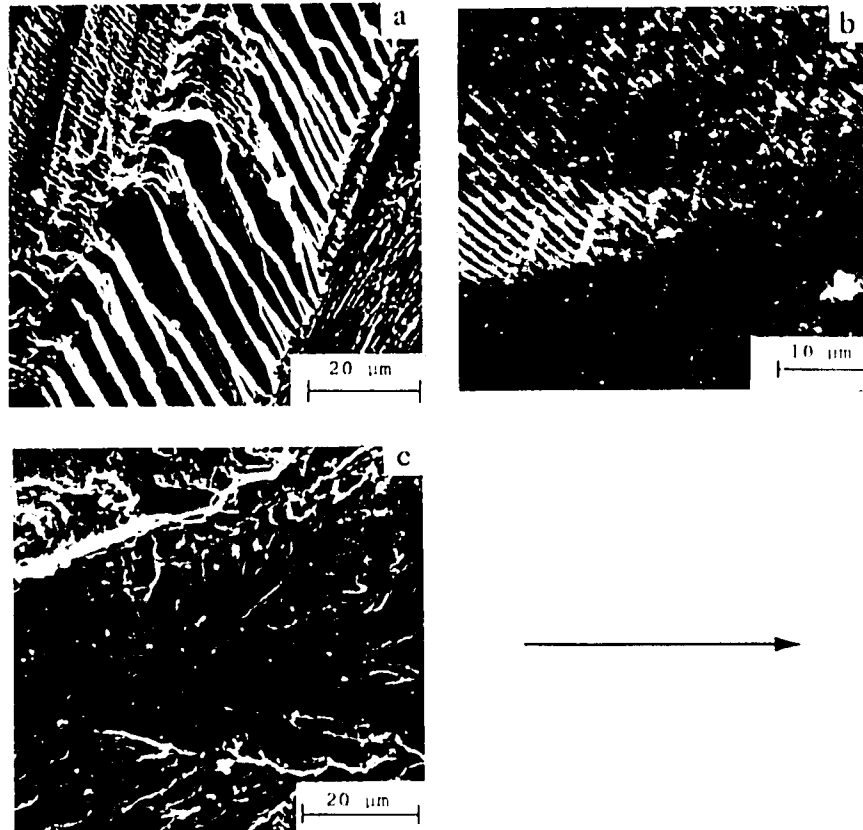


Figure 16: Three components of the FSM for beta-annealed Ti-6Al-4V alloy tested in 3.5% NaCl solution: (a) fluted facets, (b) fine striations, and (c) quasi-cleavage with small amount of ductile tearing ($\Delta K = 32 \text{ MPa-m}^{1/2}$, $R = 0.3$).

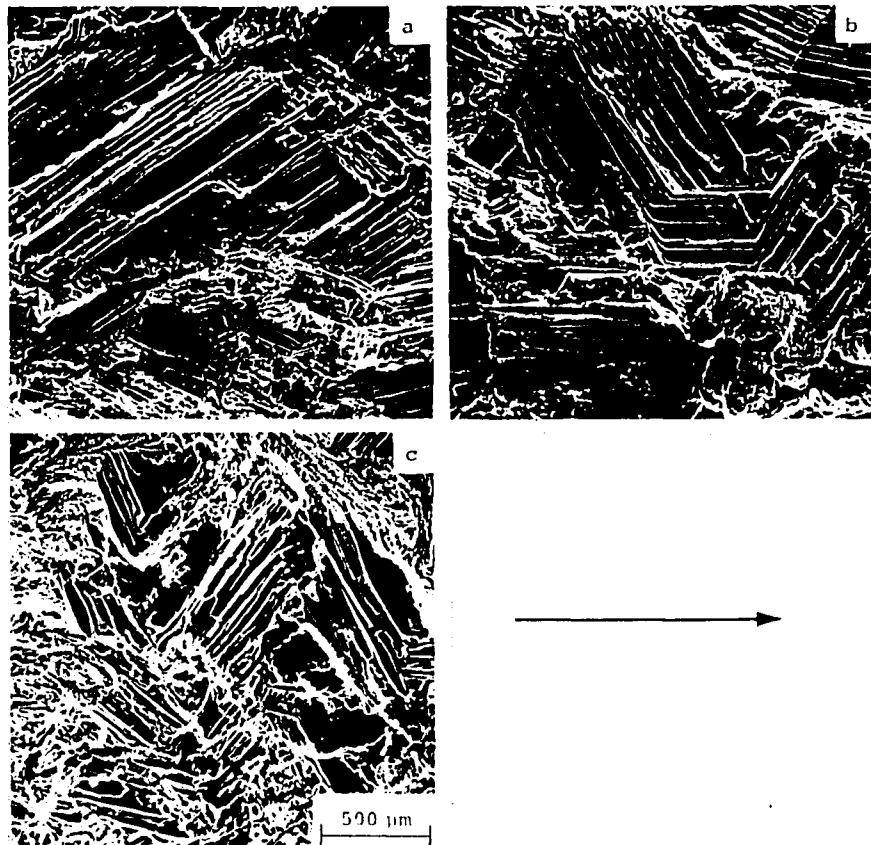


Figure 17: SEM fractographs of beta-annealed Ti-6Al-4V alloy tested in 3.5% NaCl solution, showing similar fracture morphology at critical growth rates, (a) $\Delta K = 27 \text{ MPa-m}^{1/2}$ at $f = 10 \text{ Hz}$, (b) $\Delta K = 30 \text{ MPa-m}^{1/2}$ at $f = 3 \text{ Hz}$, and (c) $\Delta K = 44 \text{ MPa-m}^{1/2}$ at $f = 0.3 \text{ Hz}$.

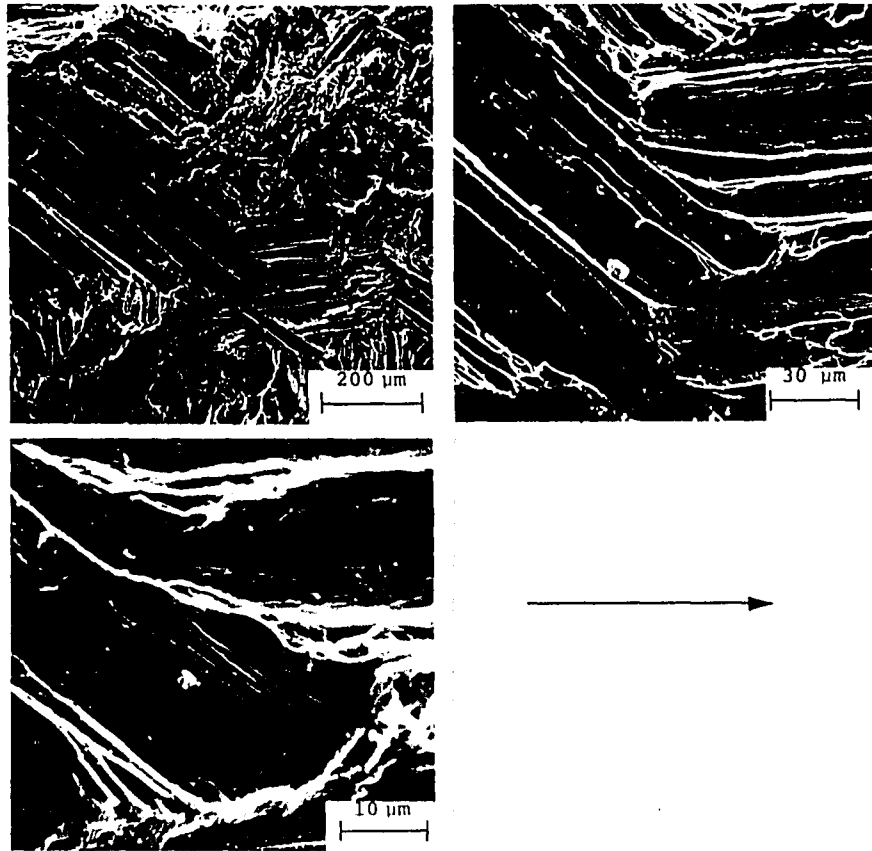


Figure 18: SEM fractographs of the fluted component of beta-annealed Ti-6Al-4V alloy tested in 3.5% NaCl solution at three different magnifications ($\Delta K = 32 \text{ MPa-m}^{1/2}$, $f = 0.03 \text{ Hz}$, and $R = 0.3$).

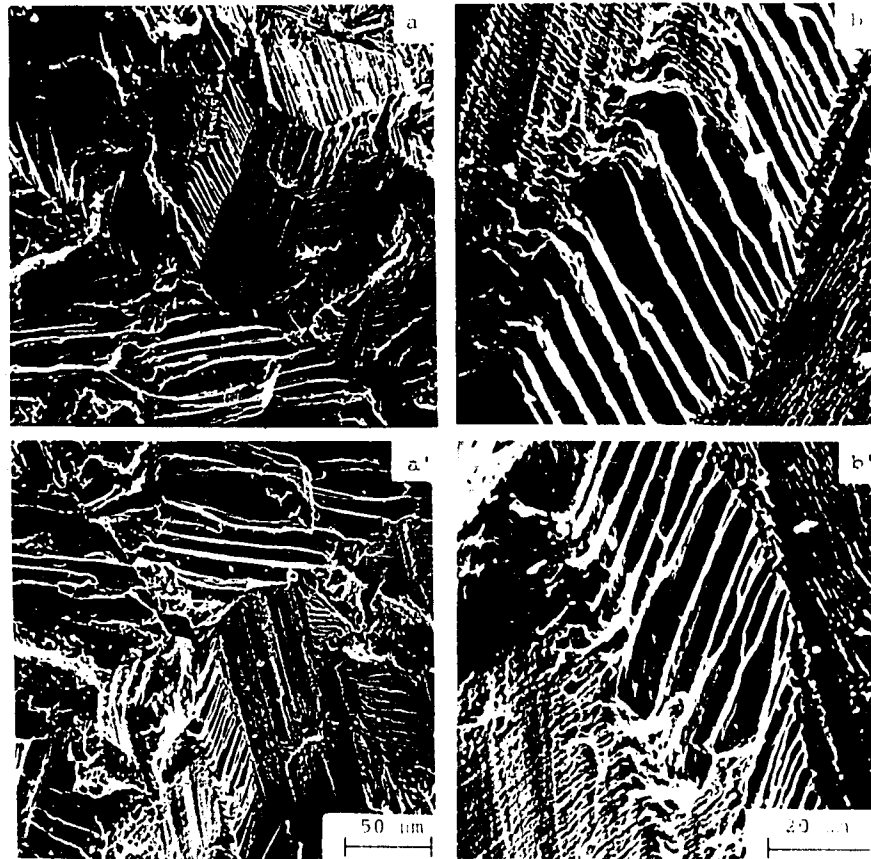


Figure 19: SEM micrographs from mating fracture surfaces of beta-annealed Ti-6Al-4V alloy tested in 3.5% NaCl solution, showing the features of fluted component ($\Delta K = 32 \text{ MPa-m}^{1/2}$, $f = 1 \text{ Hz}$, and $R = 0.3$); mating pairs are a-a' and b-b'.

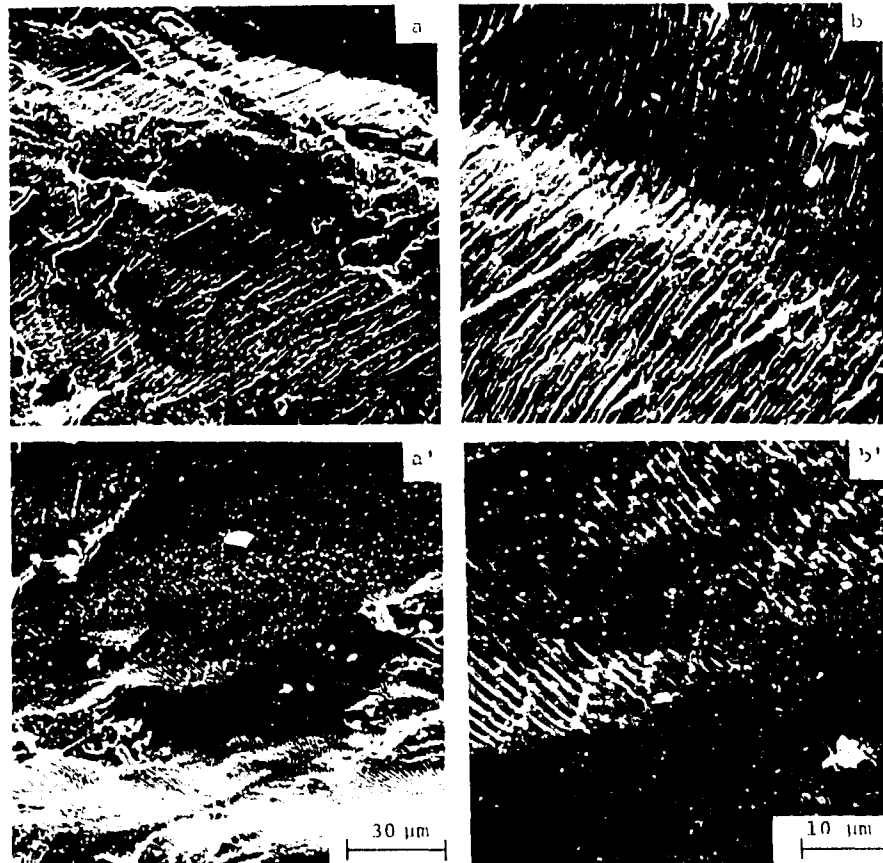


Figure 20: SEM micrographs from mating fracture surfaces of beta-annealed Ti-6Al-4V alloy tested in 3.5% NaCl solution showing the features of striation component ($\Delta K = 32 \text{ MPa-m}^{1/2}$, $f = 10 \text{ Hz}$, $R = 0.3$); mating pairs are a-a' and b-b'.

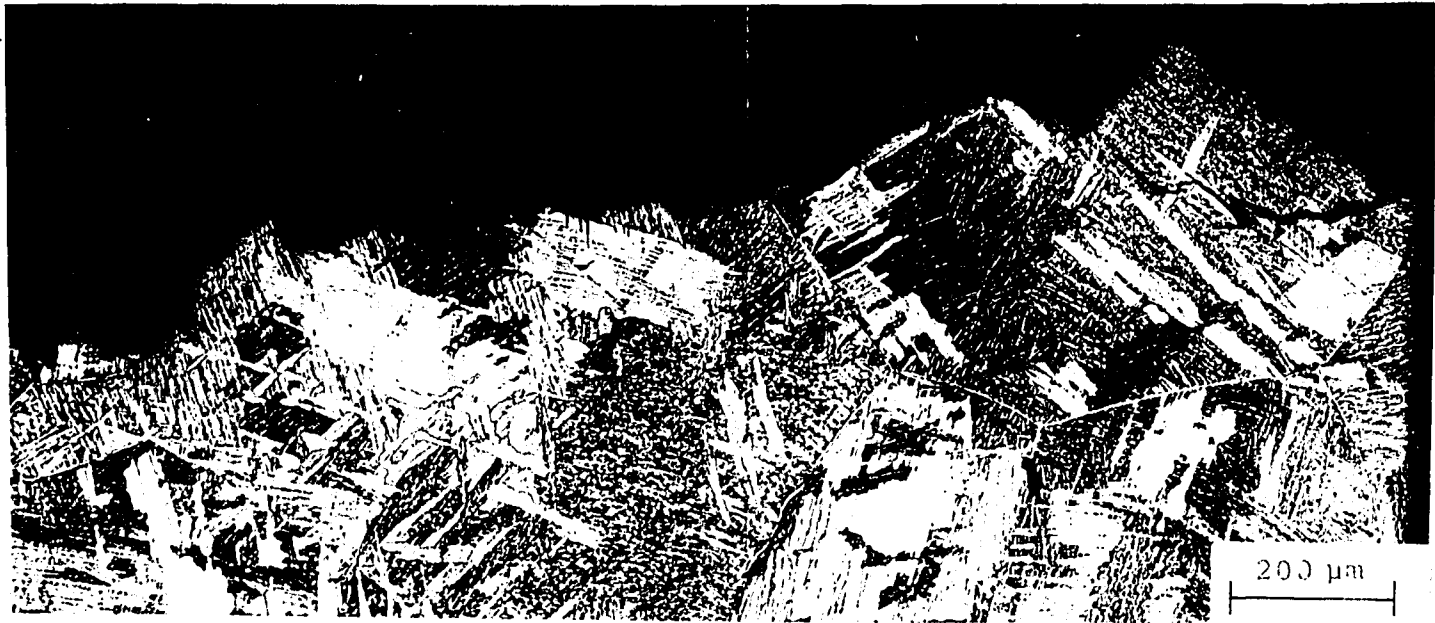


Figure 21: Fracture surface profile and the underlying microstructure of beta-annealed Ti-6Al-4V alloy tested in 3.5% NaCl solution ($\Delta K = 44 \text{ MPa-m}^{1/2}$, $f = 0.3 \text{ Hz}$, and $R = 0.05$).



Figure 21: Fracture surface profile and the underlying micro-structure of beta-annealed Ti-6Al-4V alloy tested in 3.5% NaCl solution ($\Delta K = 44 \text{ MPa}\cdot\text{m}^{1/2}$, $f = 0.3 \text{ Hz}$, and $R = 0.05$).

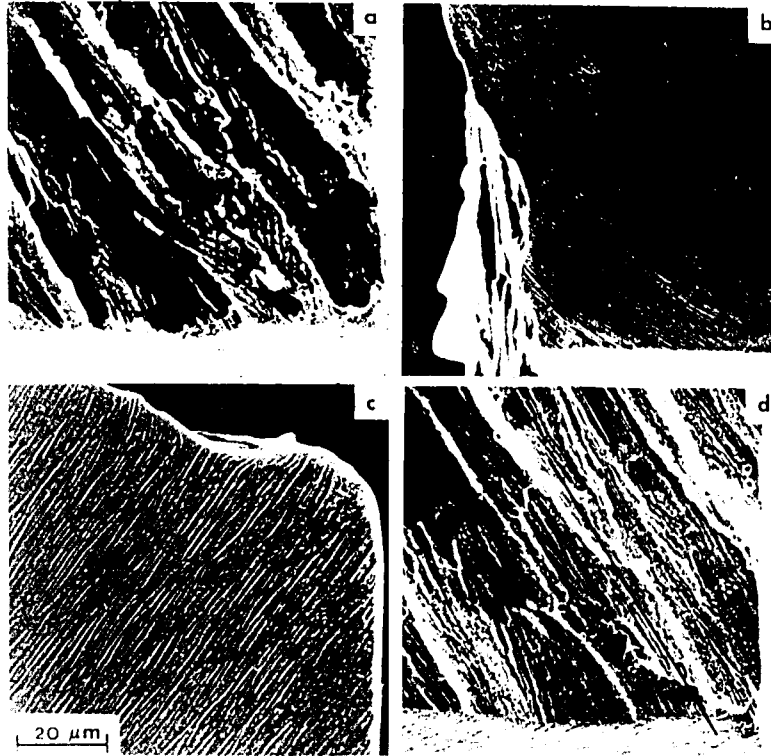


Figure 22: Fracture surface and the underlying microstructure of beta-annealed Ti-6Al-4V alloy tested in 3.5% NaCl solution ($\Delta K = 44 \text{ MPa-m}^{1/2}$, $f = 0.3 \text{ Hz}$, and $R = 0.05$): (a) fracture surface; (b) section parallel to specimen surface, (c) section transverse to crack growth direction, and (d) fracture surface after etching.

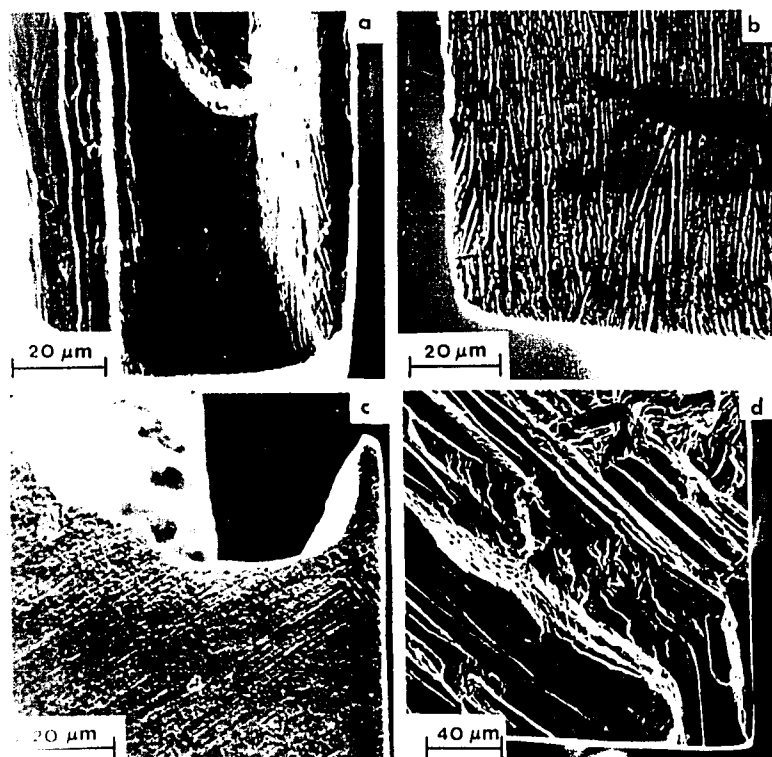


Figure 23: Fracture surface and the underlying microstructure of beta-annealed Ti-6Al-4V alloy tested in 3.5% NaCl solution ($\Delta K = 44 \text{ MPa-m}^{1/2}$, $f = 0.3 \text{ Hz}$, and $R = 0.05$): (a) fracture surface, (b) section transverse to crack growth direction, (c) section parallel to specimen surface, and (d) fracture surface at a lower magnification.

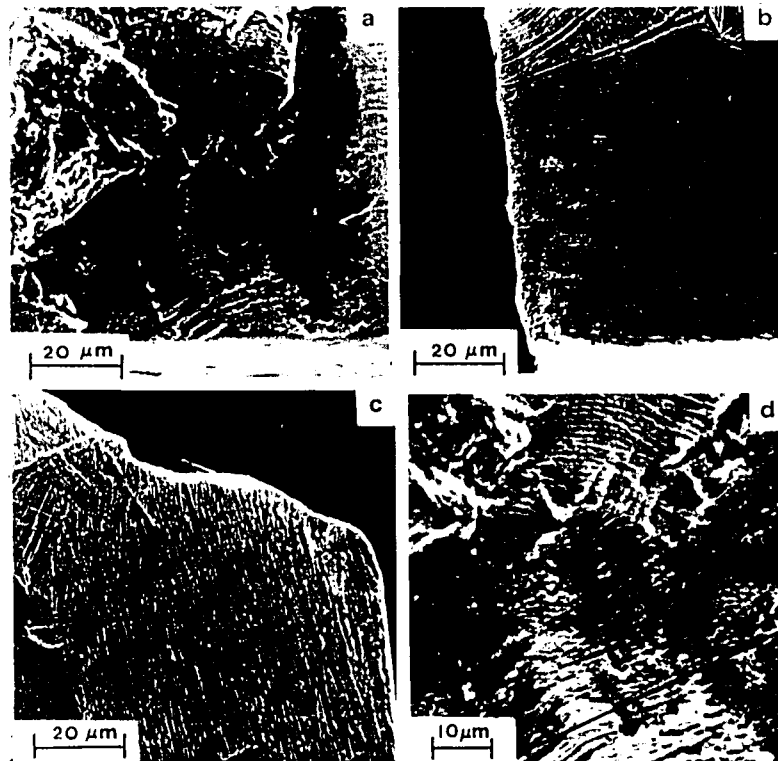


Figure 24: Fracture surface and the underlying micro-structure of beta-annealed Ti-6Al-4V alloy tested in 3.5% NaCl solution ($\Delta K = 44 \text{ MPa-m}^{1/2}$, $f = 3 \text{ Hz}$, and $R = 0.05$): (a) fracture surface, (b) section parallel to specimen surface, (c) section transverse to crack growth direction, and (d) fracture surface of a higher magnification.

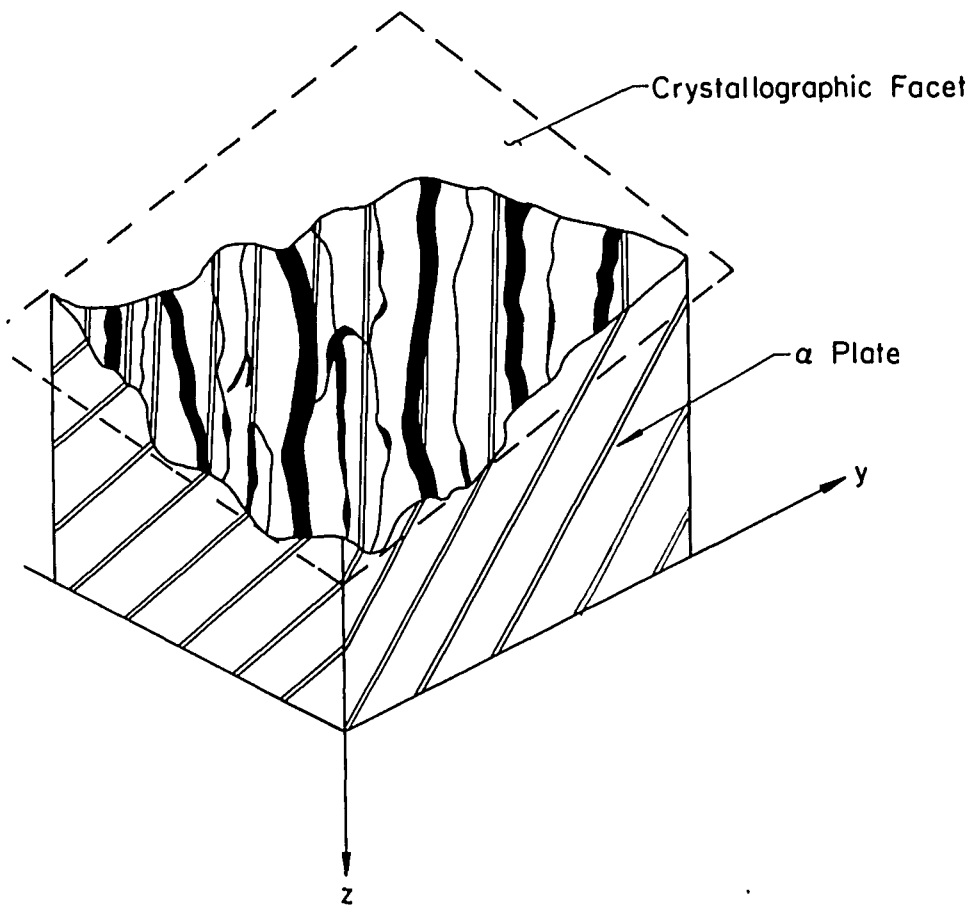


Figure 25: Schematic illustration of the fracture surface morphology with its underlying microstructure as shown in Fig. 22; angle between alpha platelets and crystallographic (fracture) facet is about 78°.

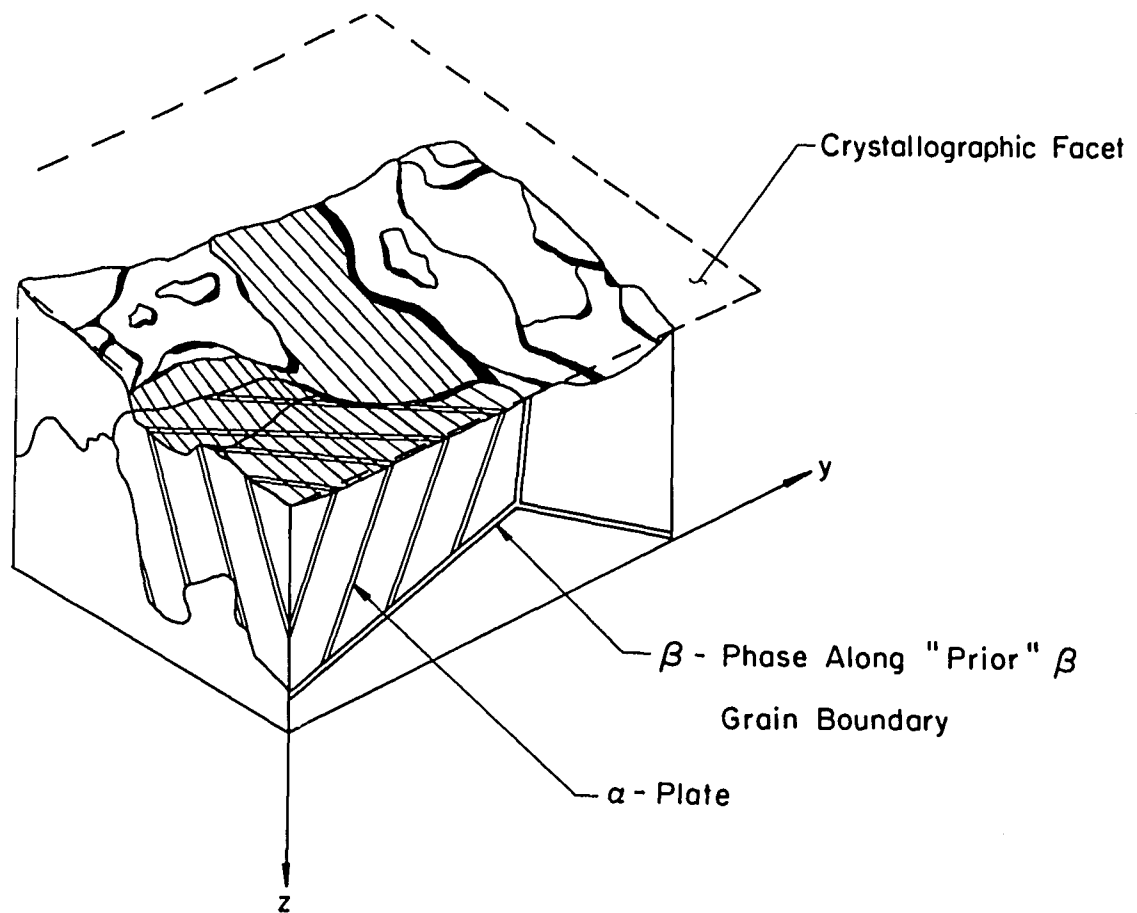


Figure 26: Schematic illustration of the fracture surface morphology with its underlying microstructure as shown in Fig. 24; angle between alpha platelets and crystallographic (fracture) facet is about 79° .

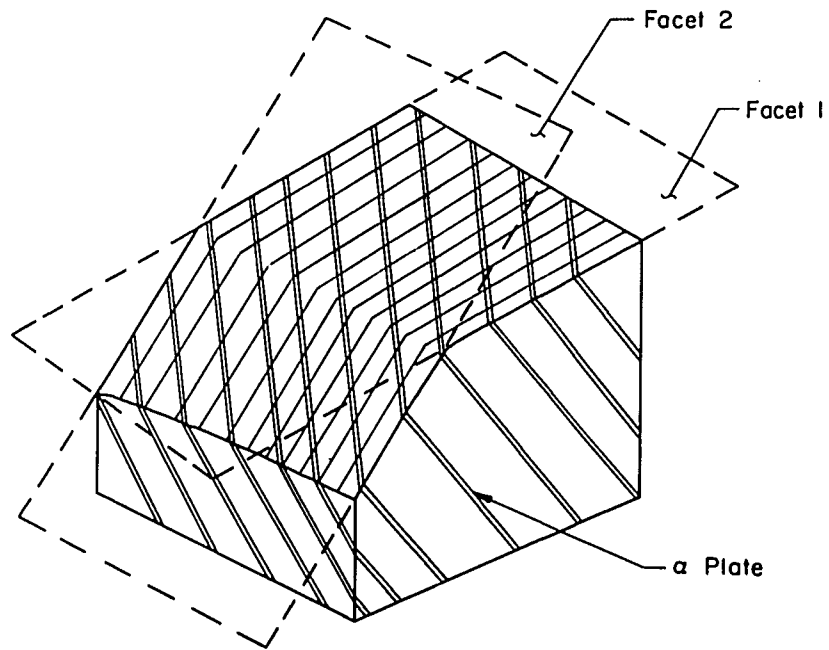


Figure 27: Schematic illustration of the fracture surface morphology with its underlying microstructure; angle between alpha platelets and crystallographic (fracture) facet is about 78°.

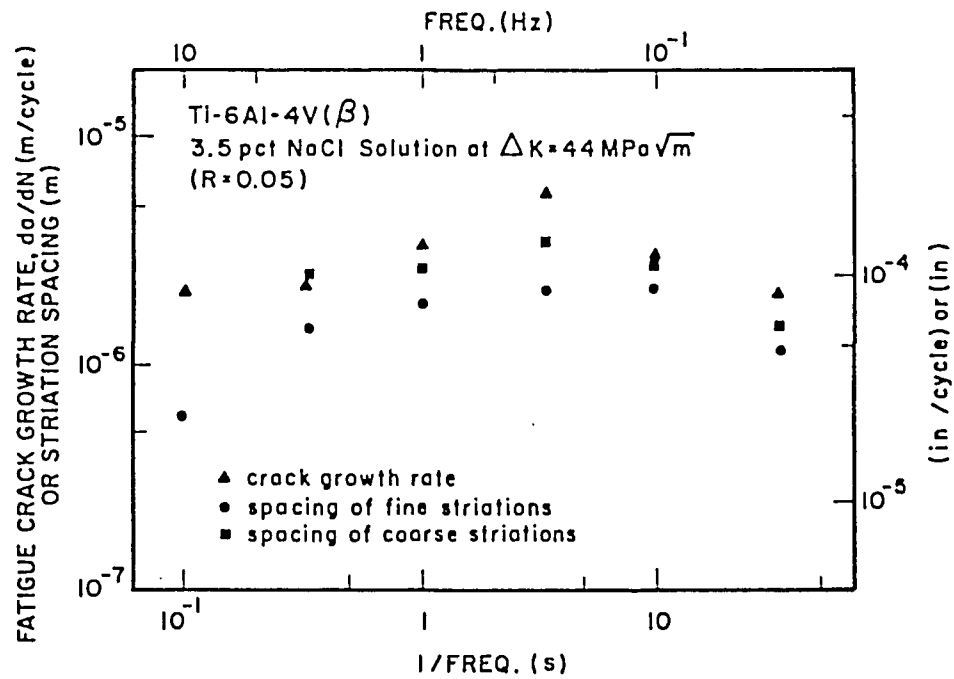


Figure 28: Comparison between striation spacings and macro crack growth rates at different frequencies.

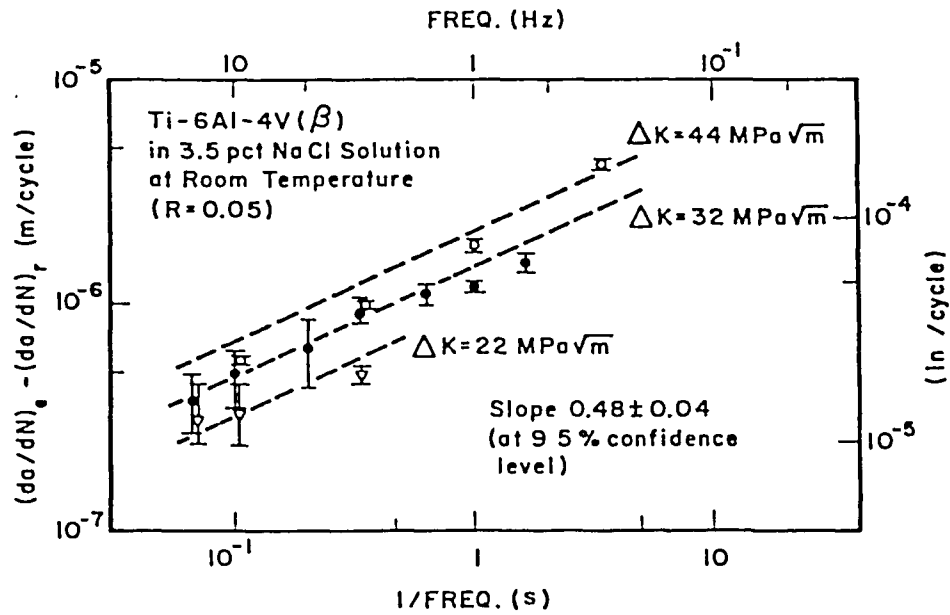


Figure 29: Relationship between $(da/dN)_{cf}$ and frequency for Ti-6Al-4V alloy tested in 3.5% NaCl solution at room temperature.

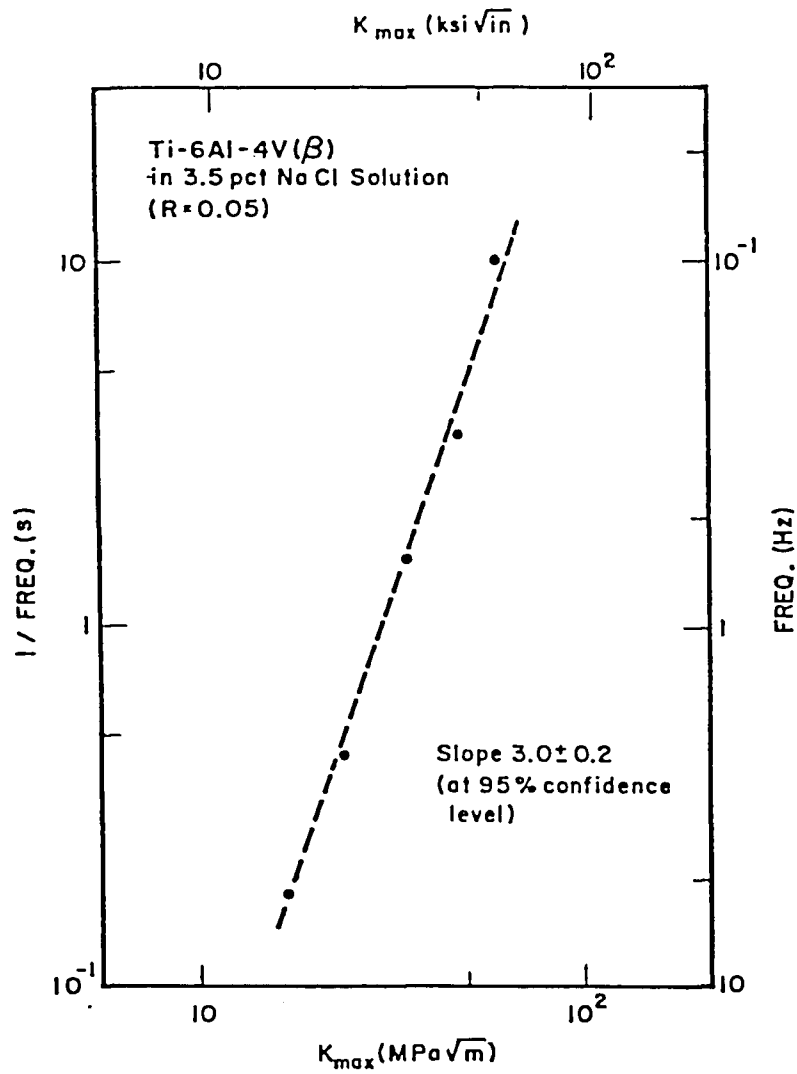


Figure 30: Relationship between K_{max} and frequency at maximum crack growth rates shown in Fig. 9.

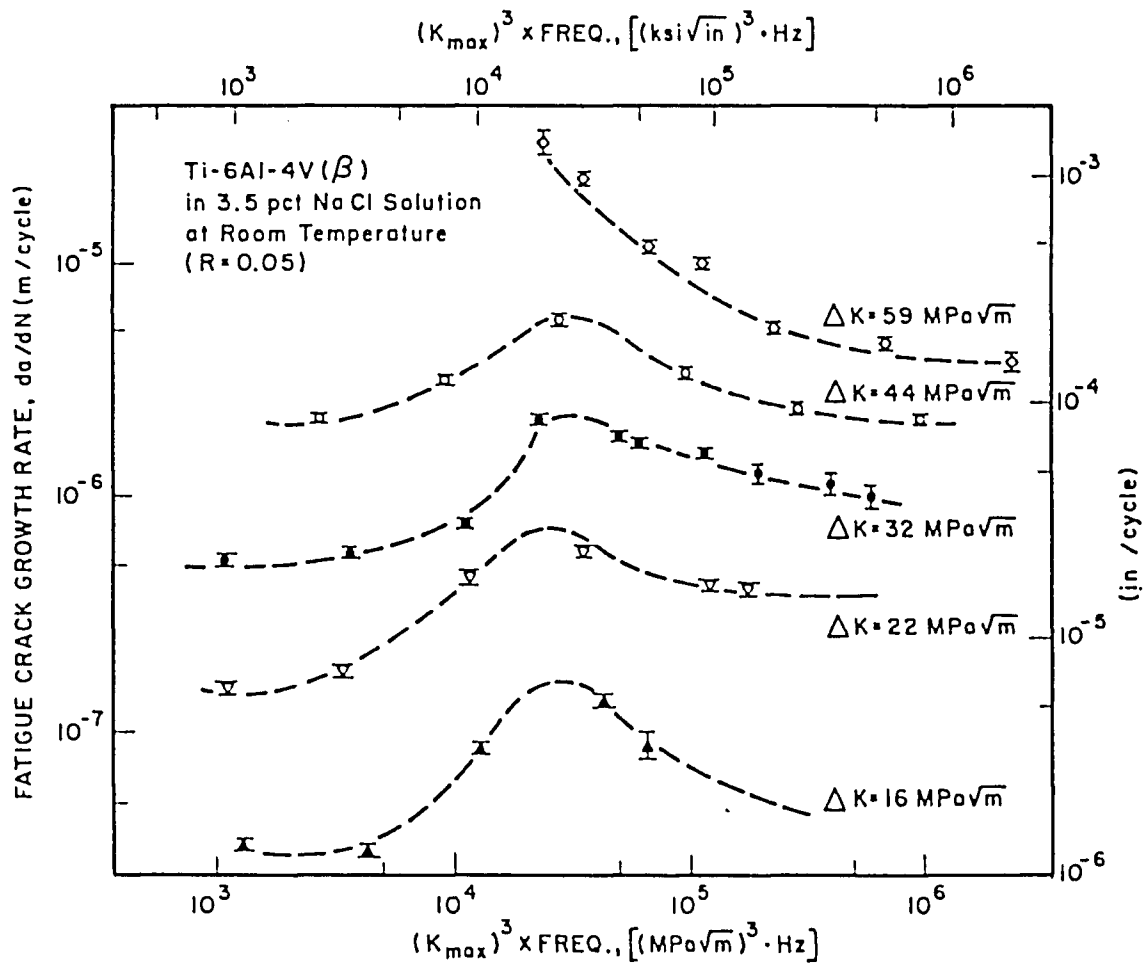


Figure 31: Fatigue crack growth response for Ti-6Al-4V alloy in 3.5% NaCl solution room temperature ($R = 0.05$) as function of the strain rate parameter $K_{max}^3 \times \text{frequency}$.

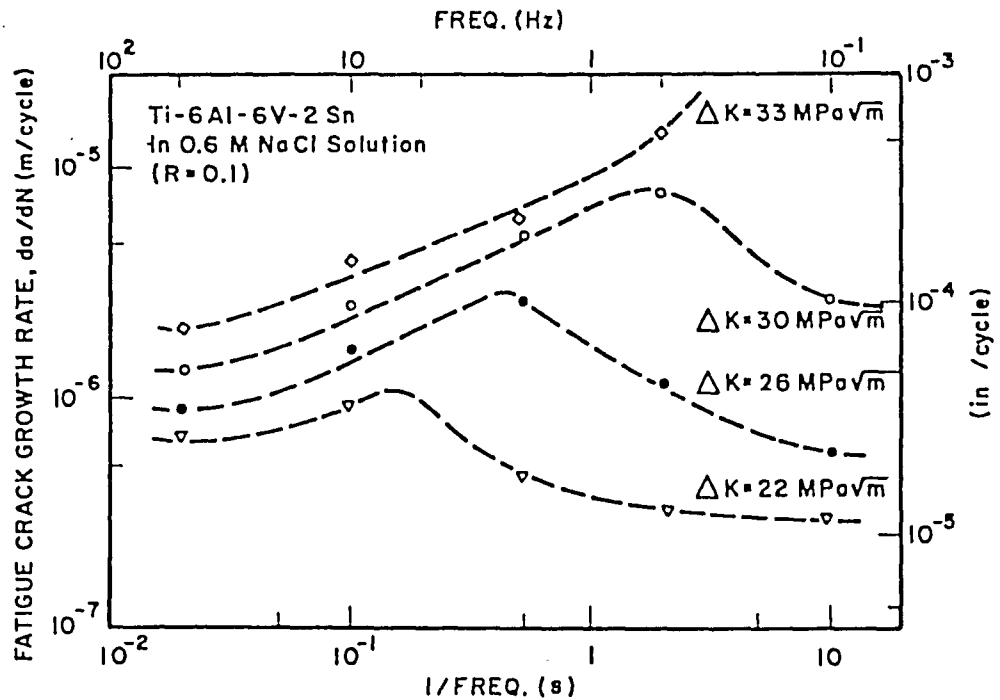


Figure 32: The influence of frequency on fatigue crack growth rate of Ti-6Al-6VSn alloy exposed to 0.6M NaCl solution (R = 0.1), by Dawson and Pelloux [11].

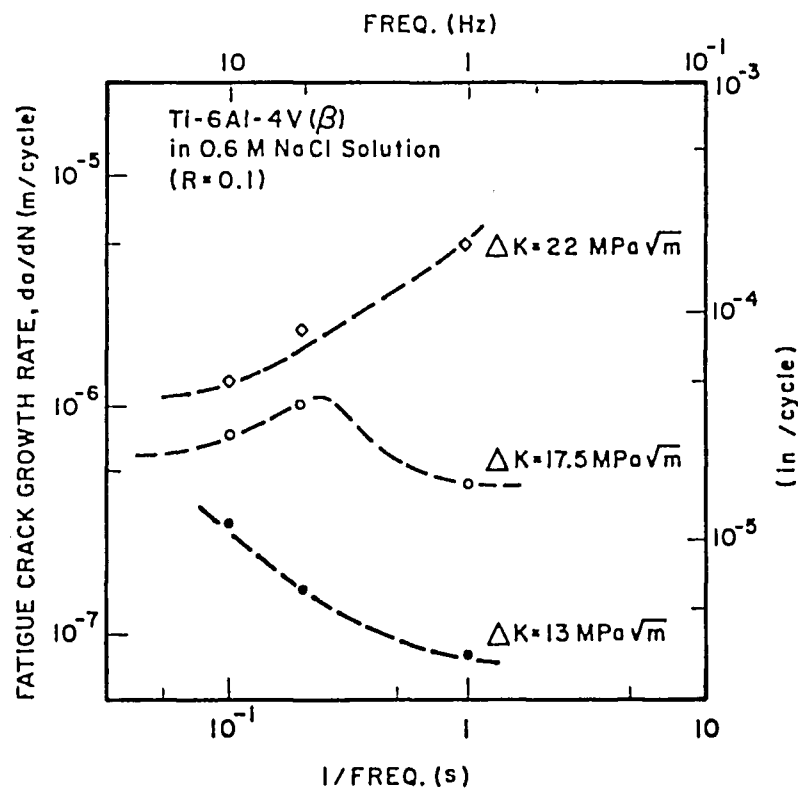


Figure 33: The influence of frequency on fatigue crack growth rate of Ti-6Al-4V alloy exposed to 0.6M NaCl solution ($R = 0.1$), by Dawson and Pelloux [11].

REFERENCES

1. D. P. Williams, P. S. Pao and R. P. Wei, "The Combined Influence of Chemical, Metallurgical and Mechanical Factors on Environment Assisted Cracking", in Environment-Sensitive Fracture of Engineering Material, Z. A. Foroulis, ed., the Met. Soc.-AIME, Warrendale, PA, (1979); p. 3.
2. R. P. Wei, P. S. Pao, R. G. Hart, T. W. Weir and G. W. Simmons, "Fracture Mechanics and Surface Chemistry Studies of Fatigue Crack Growth in an Alumium Alloy", Met. Trans. A, vol. 11A, (1980), p. 151.
3. S. J. Gao, G. W. Simmons and R. P. Wei, "Fatigue Crack arowth and Surface Reactions for Titanium Alloys Exposed to Water Vapor", to be published in J. of Materials Science and Engineering.
4. M. Lu, P. S. Pao, T. W. Weir, G. W. Simmons and R. P. Wei, "Rate Controlling Processes for Crack Growth in Hydrogen Sulfide for an AISI 4340 Steel ", Met. Trans. A, vol. 12A, (1981), p. 805.
5. R. Brazill, G. W. Simmons and R. P. Wei, "Fatigue Crack Growth in 2-1/4-Cr-1Mo Steel Exposed to Hydrogen Containing Gases", J. Eng. Matls. and Tech. vol. 101, (1979), p. 199.
6. G. W. Simmons, P. S. Pao and R. P. Wei, "Fracture Mechanics and Surface Chemistry Studies of Subcritical Crack Growth in AISI 4340 Steel", Met. Trans. A, vol. 9A, (1978), p. 1147.
7. P. S. Pao, W. Wei and R. P. Wei, "Effect of Frequency on Fatigue Crack Growth Response of AISI 4340 Steel in Water Vapor", in Environment-Sensitive Fracture of Engineering Materials, Z. A. Foroulis, ed., the Met. Soc.-AIME, Warrendale, (1979), p. 565.

8. M. Lu, P. S. Pao, N. H. Chan, K. Klier and R. P. Wei, "Hydrogen Assisted Crack Growth in AISI 4340 Steel", in Hydrogen in Metals, Suppl. to Trans. Jpn. Inst. Metals, vol. 21, (1980), p. 449.
9. N. H. Chan, K. Klier and R. P. Wei, "Hydrogen Isotope Exchange Reactions Over the AISI 4340 Steel", in Hydrogen in Metals, Suppl. to Trans. Jpn. Inst. Metals, vol. 21, (1980), p. 305.
10. T. W. Weir, G. W. Simmons, R. G. Hart and R. P. Wei, "A Model for Surface Reaction and Transport Controlled Fatigue Crack Growth", Scr. Met., vol. 14, (1980), p. 357.
11. R. P. Wei and R. L. Brazill, "An a.c. Potential System for Crack Length Measurement", in The Measurement of Crack Length and Shape during Fracture and Fatigue, C. J. Beevers, ed., Engineering Materials Advisory Services Ltd. (EMAS), Warley, England, (1980).
12. R. J. H. Wanhill, "Environment and Frequency Effect during Fatigue Crack Propagation in Ti-2.5Cu (IMI 230) Sheet at Room Temperature", Corrosion NACE, vol. 30, (1974), p. 28.
13. D. A. Meyn, "An Analysis of Frequency and Amplitude Effects on Corrosion Fatigue Crack Propagation in Ti-8Al-1Mo-1V", Met. Trans. A, vol. 2, (1971), p. 853.
14. D. B. Dawson and R. M. Pelloux, "Corrosion Fatigue Crack Growth of Titanium Alloy in Aqueous Environments", Met. Trans. A, vol. 5, (1974), p. 723.
15. R. J. Bucci, "Environment Enhanced Fatigue and Stress Corrosion Cracking of a Titanium Alloy Plus Simple Model for the Assessment of Environment Influence on Fatigue", Ph. D. Thesis, Lehigh University, (1970).

16. H. Döker and D. Munz, "Influence of Environment on the Fatigue Crack Propagation of Two Titanium Alloys", Proc. Conf. on The Influence of Environment on Fatigue, The Institution Of Mechanical Engineering, (1977), p. 123.
17. H. G. Nelson, "A Film-Rupture Model of Hydrogen-Induced, Slow Crack Growth in Acicular Alpha-Beta Ti", Met. Trans. A, vol. 7A, (1976), p. 621.
18. M. J. Blackburn and J. C. Williams, "Fundamental Aspects of Stress Corrosion Cracking", NACE, Houston, (1969), p. 620.
19. P. S. Pao and G. W. Wille, "Effect of Hydrogen on Flaw Growth in Ti-6Al-2Sn-4Zr-2Mo-0.1Si", J. Nuclear Materials, vol. 103 and 104, (1981), p. 931.
20. Y. H. Kim, D. E. Gordon, S. M. Speaker, S. D. Manning and R. P. Wei, "Development of Fatigue and Crack Propagation Design and Analysis Methodology in a Corrosive Environment for Typical Mechanically-Fastened Joints", General Dynamic/FortWorth contract no. N62269-81-c-0268, to be issue.
21. J. E. Srawley, "Wide Range Stress Intensity Factor Expressions for ASTM E399 Standard Fracture Toughness Specimens", International J. of Fract. Mechanics, vol. 12, (1976), p. 475.
22. D. Broek and J. Schijve, "The Influence of Mean Stress on the Propagation of Fatigue Cracks in Aluminum Alloy Sheet", National Aerospace Institute Amsterdam, Tr-M-211, (1963).
23. T. H. Shih and R. P. Wei, "The Effects of Load Ratio on Environmentally Assisted Fatigue Crack Growth", Engr. Frac. Mech., (1983), p. 827.

24. D. A. Meyn and E. J. Brooks, "Microstructural Origin of Flutes and Their Use in Distinguishing Striationless Fatigue Cleavage from Stress Corrosion Cracking in Titanium Alloys", Fractography and Material Science, ASTM STP 733, L. N. Gilbertson and R.D. Zipp, Eds, ASTM, (1981), p. 5.
25. W. J. Evans and C. R. Gostelow, "The Effect of Hold Time on the Fatigue Properties of a Beta-Processed Titanium Alloy", Met. Trans. A, vol. 10A, (1979), p. 1837.
26. I. Aitchison and B. Cox, "Technical Note Interpretation of Fractographs of SCC in Hexagonal Metals", Corrosion-NACE, vol. 28, no. 3, (1972), p. 83.
27. R. P. Wei, "Rate Controlling Process and Crack Growth Response", in Hydrogen Effect in Metals, eds. by I. M. Bernstein and Anthony W. Thompson, (1981), p. 677.
28. William W. Gerberich, "Hydrogen Metals", I. M. Bernstein eds., ASM Metal Park, (1973), p. 115.
29. R. P. Wei and G. W. Simmons, "Surface Reactions and Fatigue Crack Growth", in Fatigue: Environment and Temperature Effects, eds. John J. Burke and Weiss Sagamore, Army Materials Research Conference Proceeding, vol. 27, (1983), p. 59.
30. K. P. Peterson, J. C. Schwanebeck and W. W. Gerberich, "In Site Scanning Auger Analysis of Hydrogen-Induced Fracture in Ti-6Al-2Sn", in Met. Trans. A, (1978), p. 1169.
31. P. S. Pao, R. J. Lederich and S. M. L. Sastry, "Hydrogen-Assisted Crack Growth in Ti Alloy", in Micro and Macro Mechanics of Crack Growth, eds. K. Sadana, B. B. Rath and D. J. Michel. AIME Warrendale, (1982), p. 71.
32. Pao. and J. E. O'Neal, "Hydrogen Enhanced Fatigue Crack Growth in Ti-6242S", to be published.

33. D. Eylon, "Faceted Fracture in Beta-Annealed Titanium Alloy", Meta. Trans. A, vol. 10A, (1979), p. 311.
34. D. Schechtman and D. Eylon, "On the Unstable Shear in Fatigued Beta-annealed Ti-11 and IMI 685 Alloy", Met. Trans. A, (1978), p. 1018.
35. C. C. Wojcik, M.Sc. Thesis, Michigan Technological University, (1977).
36. J. D. Boyd, "Deformation-Assisted Nucleation of Titanium Hydride in an Alpha-Beta Titanium Alloy", the Science, Technology and Application of Titanium, R. T. Jaffee and N. E. Promisel eds. (1970), p. 545.
37. D. N. William, "The Hydrogen Embrittlement of Titanium Alloys", Journal of the Institute of Metals, (1962-63), p. 147.
38. V. A. Livanov, B. A. Kolachev, and A. A. Buhanova, "Hydrogen Embrittlement of Titanium and Its Alloy", the Science, Technology and Application of Titanium, R. I. Jaffee, and N. E. Promisel, (1970), p. 561.
39. Howard G. Nelson, Dell P. Williams and James E. Stein, "Environment Hydrogen Embrittlement of an Alpha-Beta Titanium Alloy : Effect of Microstructure", Met. Trans. A, (1972), p. 469.
40. J. D. Boyd, "Precipitation of Hydrides in Titanium Alloy", Trans. of ASM, (1969), p. 977.
41. G. A. Lenning, C. M. Craighead and R. I. Jaffee, "Constitution and Mechanical Properties of Titanium-Hydrogen Alloy", Journal of Metal, (1954), p. 367.
42. C. M. Craighead, G. A. Lenning and R. I. Jaffee, "Hydrogen Embrittlement of Beta-Stabilized Titanium Alloy", Journal of Metal, (1956), p. 923.

43. J. W. Hutchinson, "Plastic Stress and Strain Fields at a Crack Tip", Journal of Mechanics Physics of Solids, (1968), p. 337.
44. P. D. Hilton and J. W. Hutchinson, "Plastic Intensity Factors for Cracked Plates", Engineering Fracture Mechanics, (1971), p. 435.
45. J. R. Ambrose and J. Kruger, "Tribo-Ellipsometric Study of the Repassivation Kinetics of A Ti-8Al-1Mo-1V Alloy", Journal of the Electrochemical Society, (1974), p. 599.
46. T. R. Beck, "Stress Corrosion Cracking of Titanium Alloys", Journal of Electrochemical Society, vol. 115, no. 9, (1968), p. 890.

APPENDIX I

Calculation of the Angle Between $\{10\bar{1}0\}$ and $(10\bar{1}7)$

Based on the geometrical relationship between crystal planes in a hexagonal lattice, the angle ϕ between the plane $(h_1 k_1 i_1 l_1)^*$ and the plane $(h_2 k_2 i_2 l_2)^*$ can be expressed by the following equation.

$$\cos \phi = \frac{h_1 h_2 + k_1 k_2 + \frac{1}{2}(h_1 k_2 + h_2 k_1) + \frac{3a^2}{4c^2} l_1 l_2}{\sqrt{(h_1^2 + k_1^2 + h_1 k_1 + \frac{3a^2}{4c^2} l_1^2)(h_2^2 + k_2^2 + h_2 k_2 + \frac{3a^2}{4c^2} l_2^2)}}$$

where

a and c are lattice parameters.

The habit plane of titanium hydride has been shown to be $(10\bar{1}7)$ [18]. It is also known that the orientations of alpha-platelets are nearly parallel to the $\{10\bar{1}0\}$ prismatic planes [33,34,35]. For pure titanium, the ratio of a/c is 1/1.588. Then, the angles ϕ between $(10\bar{1}7)$ and $\{10\bar{1}0\}$ can be obtained as follows:

Crystallographic Plane	ϕ
$(10\bar{1}0)$	75.34°
$(01\bar{1}0)$	75.34°
$(\bar{1}100)$	97.2° or 82.8°

* The indices of a plane in the hexagonal system are written $(h k i l)$. The value of i depends on the values of h and k. The relation is

$$h + k = -i$$

VITA

Song Chiou was born in Taichung, Taiwan, on March 20, 1958, the son of Shi-An Chiou and Tsai-Chuan Chen Chiou. He received his primary and secondary education in Taichung, Taiwan. He graduated from National Central University, with a Bachelor of Science degree in Mechanical Engineering in August, 1981.

In September 1981, he began his graduate studies at Lehigh University. Since then, he has studied under the supervision of Professor R. P. Wei for the degree of Master of Science in Applied Mechanics. Preliminary results of his thesis research were presented at the TMS-AIME Annual meeting in Atlanta, GA, March, 1983.